1

Micro/Nanostructured Materials from Droplet Microfluidics

Xin Zhao[1], *Jieshou Li*[1], *and Yuanjin Zhao*[1,2]

[1] *Medical School of Nanjing University, Research Institute of General Surgery, Jinling Hospital, No. 305, East Zhongshan Road, Xuanwu District, Nanjing 210002, P. R. China*
[2] *Southeast University, State Key Laboratory of Bioelectronics, School of Biological Science and Medical Engineering, No. 2, Sipailou, Xuanwu District, Nanjing 210096, P. R. China*

1.1 Introduction

Since the emergence of microfluidics at the beginning of 1980s, microfluidic technologies have been extensively applied in the fabrication of materials with specific physicochemical features and versatile applications [1–3]. This relatively new field is the synergy of science and technology of systems with integrated channels on the microscale dimensions, through which small quantities of fluids (usually 10^{-9} to 10^{-18} l) can flow in designed configurations and are precisely controlled and manipulated [4–6]. In the field of microfluidics, as fluid dimensions shrink to the microscale level, their specific surface area increases, thus showing behaviors divergent from those of macroscopic fluids, which can be characterized by three major phenomena: highly efficient mass–heat transfer, relative dominance of viscous force over inertial force, and significant surface effects [7, 8]. In addition, the high integration of microfluidic channels facilitates the coexistence and diverse interactions of multiple fluid phases and paves the way for miniaturized systematic control over individual fluids and fluid interfaces [9, 10]. These features offer obvious advantages over bulk synthesis, most notably in their ability to ensure monodispersity and control the structure of final products [11–13]. Therefore, microfluidics has promoted the development of multidisciplinary research in physical, chemical, biological, medical, and engineering fields.

Droplet microfluidics is an important subcategory of the microfluidic technologies, which generates and manipulates discrete droplets through immiscible multiphase flows inside the microchannels [14–16]. In the past two decades, fostered by great progress in both theoretical and technical aspects, droplet microfluidics has fulfilled original expectations and become a significant approach to generate materials for a broad range of applications [17–19]. The basic principles and microfluidic devices for droplet generation are shown

Nanotechnology and Microfluidics, First Edition. Edited by Xingyu Jiang.

in Figure 1.1, including a T-junction chip (Figure 1.1a), a flow-focusing chip (Figure 1.1b), and a coaxial structured chip (Figure 1.1c) [20]. In the T-junction chip, the dispersed phase flows from a vertical channel to a horizontal channel filled with the continuous phase. Under the combined action of both shear force and extrusion pressure from the continuous phase, monodispersed droplets are generated. In the flow-focusing chip, the dispersed phase flows from the middle channel and undergoes extrusion force of the continuous phase from all directions. The dispersed phase experiences stretching and breakage, leading to droplet formation. In the coaxial structured chip, the dispersed phase channel is embedded in the continuous phase channel, and the dispersed phase flows parallel to the continuous phase toward the same direction. Also, the dispersed phase is broken into droplets. In microfluidic systems, droplet generation is influenced by microchannel construction, viscosity and flow velocity of each phase, and interfacial tension between adjacent flows. Therefore, the dimensions and production rates of droplets can be regulated by adjusting the above parameters. In addition, through a flexible design of microchannels, double or even multiple emulsions could be generated in a controlled manner (Figure 1.1d,e) [21, 22]. These microfluidic droplets have diverse morphologies and components and can serve as excellent templates to synthesize materials with specific structures and functions.

With the development of microfabrication technology, considerable research has been made to synthesize microstructured materials (MMs)/nanostructured materials (NMs) because the microscopic architectures give additional properties to the materials [23–26]. Conventional bulk methods usually adopt a certain physical or chemical procedure (e.g. mechanical stirring) [27, 28]. These methods usually generate materials with a monotonous morphology, and the dispersity of products and synthetic processes are difficult to control [29, 30]. In particular, for fabrication of composite materials, such as "intelligent materials" or "core–shell materials," the conventional approaches are insufficient to meet the requirements. MMs/NMs synthesized from droplet microfluidics possess narrow size distribution, flexible structures, and desired properties [31–33]. Compared to conventional methods, the advantages of microfluidic synthesis lie in the following aspects [20, 34–36]. The material size, structure, and composition are easily controlled, resulting in superior properties and functions. The addition of reagents is very simple, which is beneficial for the manipulation of multistep and multireagent synthesis. Through scale integration of microfluidic systems and equipment automation, the complex reaction process can be largely simplified. Because majority of materials used to make microfluidic chip are facilitated to be observed, real-time monitoring of the reaction process could be realized, which helps to clarify the synthesis mechanism. Therefore, the application of droplet microfluidics to design and prepare MMs/NMs has become a hot topic recently and will bring about infinite possibilities for the future development of materials science.

In this chapter, we summarize the classical and recent achievements in the MMs/NMs engineered from droplet microfluidics and their various applications. We first provide an overview of MMs fabricated by droplet microfluidics, including the droplet formation mechanism and various microchips used to

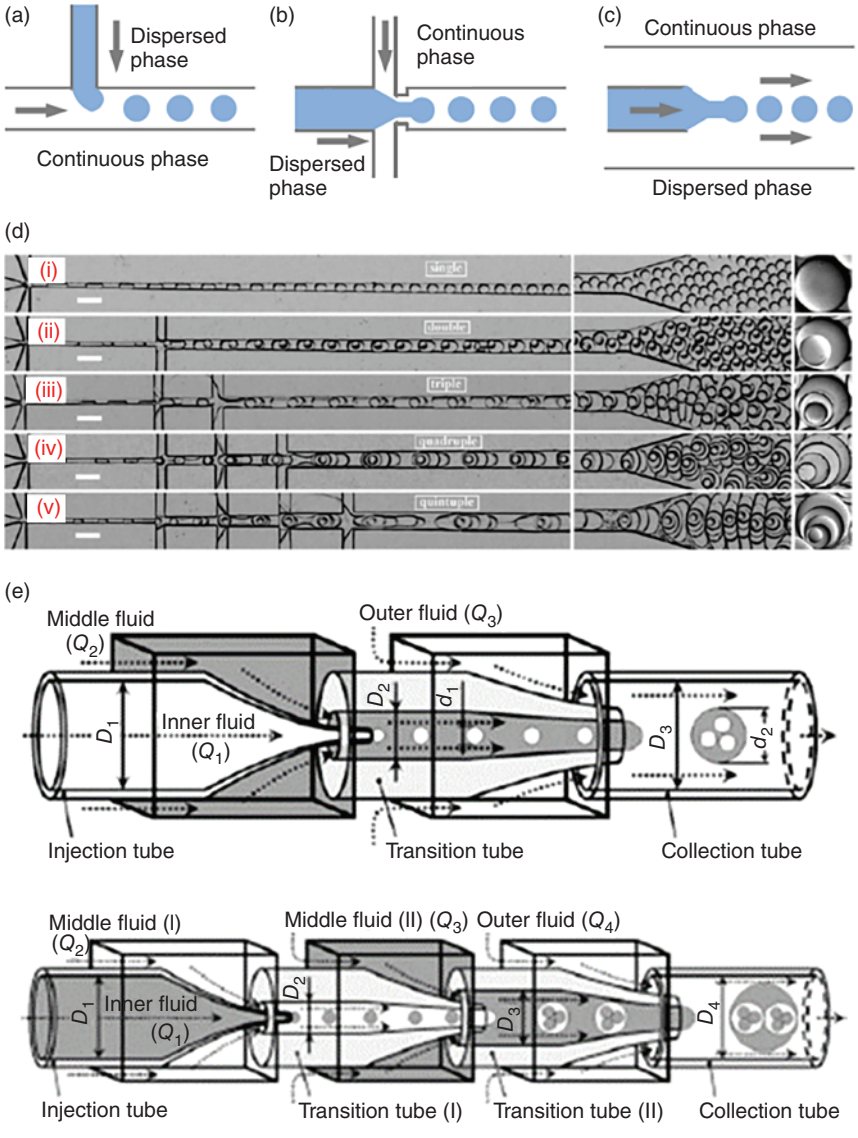

Figure 1.1 (a–c) The principles and chip designs with different flow regimes for droplet generation, including T-junction (a), flow-focusing (b), and coaxial (c) structured chip. Source: Ma et al. 2017 [20]. https://www.mdpi.com/2072-666X/8/8/255. Licensed under CCBY 4.0 (d) Generation of multiple emulsions in a stepwise flow-focusing device: (i–v) single-, double-, triple-, quadruple-, and quintuple-emulsion droplets, respectively. Source: Adapted with permission from Abate and Weitz [21]. Copyright 2009, John Wiley & Sons. (e) Generation of multiple emulsions in a stepwise coflow platform. Source: Adapted with permission from Chu et al. [22]. Copyright 2007, John Wiley & Sons.

generate different droplets, the methods to prepare MMs templated from these droplets, and the unique and complex structures enabled by microfluidic techniques. We then present basic synthesis methods for inorganic and organic NMs through droplet microfluidics, and the heterogeneous and multifunctional nanostructures from microfluidic platforms are also introduced. Following these two sections, much emphasis will be laid on the applications of the generated MMs/NMs, including drug delivery, cell encapsulation, TE, and analytical applications. Finally, we will discuss the current status and existing challenges and provide opinions on the directions of future development of droplet microfluidics in the synthesis of advanced MMs/NMs.

1.2 MMs from Droplet Microfluidics

Although the history of MMs with sizes ranging from 1 to 1000 μm has started in the 1960s, their application was only expanded recently after they were utilized as drug delivery agents by mimicking genetic materials carrying pollens [37–39]. Thereafter, other studies have continuously investigated the functionalities of MMs and they are now being utilized in various fields including pharmaceuticals, food industry, cosmetics, photonics, coatings, and printing [40, 41]. These applications of MMs depend on their properties that correlate with their size, structure, composition, and configuration [42, 43]. Typically, MMs have been prepared through traditional methods including emulsion polymerization, dispersion polymerization, and spray drying [44]. These methods always result in MMs with large polydispersity, poor reproducibility, limited functionality, and less tunable morphology [44–46]. Therefore, it is becoming increasingly urgent to fabricate MMs with defined sizes, morphologies, and compartments in a controlled manner to improve their capability. Droplet microfluidics can generate emulsion droplets with a precisely controlled size, shape, and composition, which provide excellent templates for the synthesis of functional MMs with uniform size, controllable shape, and versatile compositions [47–49]. Moreover, precise control over single emulsion droplets by microfluidics allows further creation of multiple emulsions with highly controllable, nested, and droplet-in-droplet structures [50, 51]. Thus, using such multiple emulsions as templates, MMs with well-tailored internal compartments and specific functions can be successfully fabricated for many applications.

1.2.1 Simple Spherical Microparticles (MPs)

Simple spherical microparticles (MPs) are synthesized straightforwardly by solidification of the droplet templates, which involves a chemical or physical reaction process [52–54]. Photopolymerization is one of the most prevalent chemical processes because it enables *in situ* solidification and continuous fabrication in a fast response time, which helps to determine the particle location and better control the size distribution [55, 56]. For example, Jeong et al. developed a simple and cost-effective method for the fabrication of polymeric

MPs in droplet microfluidics [57]. The polymerizable sample fluid and the immiscible nonpolymerizable sheath fluid (mineral oil) were introduced into the inlet channels of the sample and sheath flow, respectively. Both fluids were combined at the tip of the pulled micropipette (dotted area in Figure 1.2a), producing hydrogel droplets floating among the sheath stream. The separated droplets traveled through the main channel without touching the inner wall of the channel and then the hydrogel droplets were polymerized by continuous ultraviolet (UV) exposure at the unshielded area. The size of the MPs could be adjusted within the range of tens to hundreds of micrometers by changing the flow rates of the dispersed and continuous phases. This method has been extensively applied for the synthesis of a large variety of MPs by using precursors with unsaturated hydrocarbon chains.

MPs synthesized via UV irradiation are inappropriate when considering their biotoxicity and biocompatibility. In those cases, physical gelation or ionic reactions are more applicable and has been employed to synthesize many kinds of MPs [62, 63]. For example, Tan and Takeuchi described the production of monodisperse alginate hydrogel MPs using a method that combined the internal gelation method with T-junction droplet formation in microfluidic devices (Figure 1.2b) [58]. They dispersed droplets of Na-alginate solution containing $CaCO_3$ nanoparticles (NPs) in a continuous phase of corn oil at room temperature. Syringe pumps were used to infuse fluids into the microfluidic device fabricated from polydimethylsiloxane (PDMS) using soft lithography techniques. Corn oil with lecithin sheared off droplets of Na-alginate solution containing insoluble $CaCO_3$ NPs one at a time to generate an inverse emulsion with a narrow size distribution. Lecithin was added to the corn oil to stabilize the droplets against coalescence, thereby preserving the monodispersity of the droplets. In downstream, acetic acid dissolved in corn oil was introduced and mixed with oil flowing in the main stream. The acetic acid then diffused into the aqueous Na-alginate droplets, reduced pH, and released Ca^{2+} ions from the insoluble calcium complex, causing gelation. Also, they demonstrated that the gelation conditions in this approach were mild enough to encapsulate cells without loss of their viability.

The low production rate of microfluidic devices for generation of MPs has remained a key challenge to successfully translate many promising laboratory-scale results to commercial-scale production of microfluidics-generated materials [64, 65]. To address these challenges, Yadavali et al. incorporated an array of 10 260 (285×36) microfluidic droplet generators onto a 3D-etched single silicon wafer that was operated using only a single set of inlets and outlets (Figure 1.2c) [59]. The monolithic construction from a single silicon wafer obviated the alignment and bonding challenges of prior multilayer approaches and allowed high-pressure use. To demonstrate the power of this approach, they generated polycaprolactone solid MPs, with a coefficient of variation (CV) <5%, and an emulsion production rate that results in 277 g/h particle production. A key to achieving this throughput lies in the design strategy that broke the tradeoff between the number of integrated droplet generators and the maximum throughput of each droplet generator. Because the device allowed

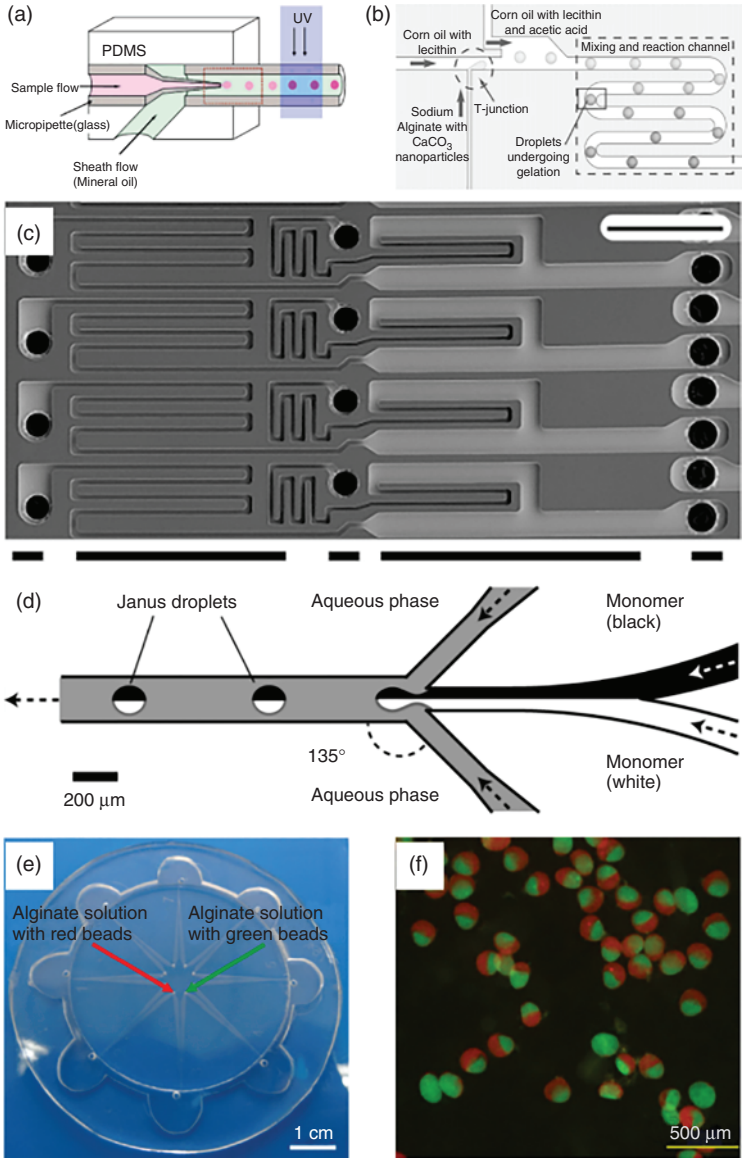

Figure 1.2 (a) MP synthesis through UV-induced photopolymerization. Source: Adapted with permission from Jeong et al. [57]. Copyright 2005, American Chemical Society. (b) Synthesis of alginate MPs through the physical cross-linking process. Source: Adapted with permission from Tan and Takeuchi [58]. Copyright 2007, John Wiley & Sons. (c) Droplet generator design for high-throughput emulsion generation. Source: Yadavali et al. 2018 [59]. https://www.nature.com/articles/s41467-018-03515-2. Licensed under CCBY 4.0. (d) Formation of bicolored Janus droplets in a planar microfluidic geometry. Source: Adapted with permission from Nisisako et al. [60]. Copyright 2006, John Wiley & Sons. (e, f) Photograph of the centrifugal microfluidic chip and fluorescence image of the Janus MPs. Source: Adapted with permission from Liu et al. [61]. Copyright 2016, Elsevier.

arbitrary microfluidic droplet generators to be parallelized, it could produce higher order emulsions and particles that required multistep processing.

1.2.2 Janus MPs

Janus particles, named after the ancient twofaced Roman god Janus, refer to particles with two hemispheres of different compositions. Such structural asymmetry brings about combination of different features and functionalities. Janus particles have received increasing attention because of their application values in various areas [66, 67]. Janus droplets serve as templates for direct synthesis of Janus particles through photoinduced or heat-induced polymerization, as well as ionic cross-linking [68, 69]. For example, Nisisako et al. showed a microfluidic technology to engineer monodisperse polymeric Janus particles with color anisotropies (Figure 1.2d) [60]. First, pigments of carbon black and titanium oxide were dispersed in an acrylic monomer (isobornyl acrylate, IBA) to prepare separate black and white monomers. The black and white IBAs were introduced into the Y-junction at the same volumetric flow rate to form a two-color stream. In downstream, aqueous streams containing a steric stabilizer co-flow symmetrically around the two-color stream. Droplets having black and white hemispheres were formed reproducibly by a shear-rupturing mechanism at an appropriate disperse-phase flow rate and continuous-phase flow rate. Then, monodisperse bicolored particles were synthesized outside the fluidic module by thermal polymerization of the generated Janus droplets. The two-color boundary was obscure, but these balls still had black and white hemispheres, with a CV less than 2%.

Microfluidic generation of Janus MPs was mainly based on T-junction and flow-focusing geometries. These particles were produced from the droplets generated by the breakup of the fluid because of the Rayleigh–Plateau instability. However, these methods depend strongly on the precise control over the geometries of the chips and manipulation of the flow rate of each fluid [70, 71]. Recently, centrifugal microfluidics, taking advantage of centrifugal force for particle generation, presented as an available method in manipulating the size and structure of particles and exhibited potentials in preparing particles with complex structures [72]. Liu et al. synthesized Janus MPs based on droplet templates formed by using a centrifugal microfluidic technique [61]. The centrifugal system simply consisted of a spin coater and a chip fabricated using the universal soft-lithographic technique (Figure 1.2e). By designing two channels adjacently parallel with each other, Janus alginate particles with two distinct fluorescent hemispheres could be synthesized (Figure 1.2f). In addition, the production throughput of the particles could be dramatically increased simply by arranging plenty of parallel channels on the chip.

1.2.3 Core–Shell MPs

Core–shell MPs are microscale materials composed of solid, liquid, or gas bubbles surrounded by a shell or coating. Because of the unique core–shell structure and high flexibility of material selection, these MPs could be imparted with diverse properties and functionalities such as efficient encapsulation,

controlled release, mass transfer, mechanical response, etc. [73, 74] In conventional approaches such as shear-induced sequential emulsification, core–shell MPs are fabricated with polydispersity in size and shape, which are unfavorable for practical applications [75]. Droplet microfluidics overcomes this dilemma because of its ability to fabricate uniform emulsion droplets with a precisely controlled size and morphology. In a single-emulsion system, core–shell MPs could be derived through phase separation, wettability control, interfacial reaction, and assembly [76, 77]. Also, core–shell MPs could be conveniently derived from multiple emulsion templates via different shell solidification processes such as triggered polymerization, solvent evaporation, phase transition, and dewetting [78, 79]. For example, Montazeri et al. used a flow focusing system to create core–shell MPs [80]. The microfluidic device consisted of three inlets and one outlet was made by soft lithography. In the first flow focusing part, the H_2O_2 solution as a disperse phase was introduced into the central channel. The poly(lactic-*co*-glycolic acid) (PLGA) solution entered from the second inlet and flowed into the two side channels as the continuous phase. At the junction, the PLGA solution stream splits the H_2O_2 stream, which resulted in the formation of H_2O_2 droplets. This emulsion encountered the second flow focusing part while it flowed in the central channel. At the junction, the emulsion was dispersed by a poly(vinyl alcohol) (PVA) solution as the second continuous phase, which led to the generation of a double emulsion. After extracting the solvent, core–shell structured, uniform PLGA MPs were successfully fabricated (Figure 1.3a).

To enhance the practical performances, more complex MPs with core–shell structure have been fabricated [85]. Through stepwise emulsification, double and higher order polymersomes were generated, with a shell membrane being added in each step. Ingredients encapsulated in different levels could be released in a programmed manner by sequentially rupturing the multilayer membranes [86]. For example, Amstad et al. used capillary microfluidic devices to produce monodisperse W/O/W double-emulsion drops as templates to form polymersomes (Figure 1.3b–d) [81]. The device consisted of two tapered cylindrical capillaries inserted in one square capillary. An aqueous solution of poly(ethylene glycol) (PEG) was injected as the innermost phase. A mixture of chloroform and hexane containing PEG-*b*-poly(lactic acid) (PLA) diblock copolymers was injected as the middle oil phase. To render the membranes thermoresponsive feature, poly(*N*-isopropylacrylamide) (PNIPAM)-*b*-PLGA diblock copolymers were added, and to render the membrane photoresponsive feature, dodecylthiol-stabilized gold nanoparticles (AuNPs) were added into the oil phase. An aqueous solution of PVA was injected as the outer continuous phase. The resulting double-emulsion drops were flowed through the collection capillary and collected. After the diffusion-induced dewetting process, the two amphiphiles assembled into polymersomes with AuNPs located in the bilayers (Figure 1.3e). The resultant polymersomes thus showed a thermoresponsive release behavior when the temperature was raised above the lower critical solution temperature of the PNIPAm-*b*-PLGA copolymer. Additionally, because of the photothermal feature of AuNPs, the polymersomes were endowed with a photoresponsive feature and encapsulant release capacity.

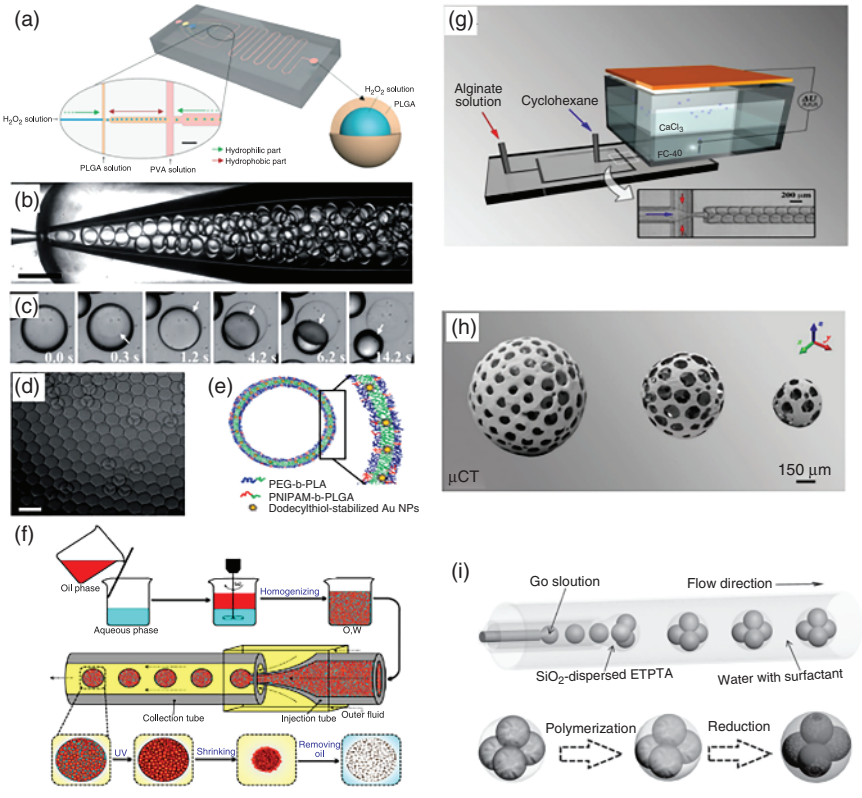

Figure 1.3 (a) Schematic presentation of the partially hydrophobic/hydrophilic chip for fabrication of the core–shell-structured MPs. Source: Adapted with permission from Montazeri et al. [80]. Copyright 2016, Royal Society of Chemistry. (b–e) Optical microscopy image showing the generation of double-emulsion drops in a capillary microfluidic device (b); a series of optical microscopy images showing dewetting of the middle phase on the surface of the innermost drop, leading to the formation of polymersomes (c); optical microscopy image of monodisperse polymersomes (scale bar = 200 mm) (d); and schematic illustration of the polymersomes (e). Source: Adapted with permission from Amstad et al. [81]. Copyright 2012, John Wiley & Sons. (f) Schematic illustration of the preparation procedure of open-celled porous PNIPAM microgels. Source: Adapted with permission from Mou et al. [82]. Copyright 2014, American Chemical Society. (g, h) Schematics of the device used for the manufacturing of porous microbeads (g); 3D reconstructions of the porous microbeads (h). Source: Adapted with permission from Costantini et al. [83]. Copyright 2018, John Wiley & Sons. (i) Schematic diagram of the capillary microfluidic device used to generate the W/O/W double and the fabrication process of the porous particles encapsulated with spongy graphene. Source: Adapted with permission from Wang et al. [84]. Copyright 2015, John Wiley & Sons.

1.2.4 Porous MPs

Porous particles are valuable because of their distinct structure and applicable for drug delivery, adsorption, sensors, etc. [87] By using droplet microfluidic techniques, porous particles could be synthesized by introducing templates into the droplet precursors and then removing them after solidification, thus generating void spaces in the particles [88]. For example, Mou et al. synthesized open-cell

porous PNIPAM microgel particles by using tiny oil drops as porogens [82]. The oil drops were first embedded in the aqueous phase of NIPAM monomers. Such a mixture was then emulsified to produce W/O emulsion droplets, which were polymerized upon UV irradiation. Afterward, by adding 2-propanol or by increasing the temperature, the embedded oil drops were squeezed out in response to volume shrinkage of the PNIPAM microgel. The resultant microgel particles were accommodated with a large number of interconnected free channels and thus showed enhanced thermal response rates compared with normal hydrogels (Figure 1.3f).

Apart from using single droplets as templates, double emulsions with multiple encapsulated inner droplets can also be used as templates for the fabrication of the porous MPs. Costantini et al. fabricated highly tailorable porous MPs by coupling a microfluidic droplet generator with a secondary breakup triggered by a pulsed electric field (EF) (Figure 1.3g) [83]. The method started with the generation of a monodisperse O/W emulsion inside a flow-focusing microfluidic device. This emulsion was later broken-up, with the use of EF, into mesoscopic double droplets, which in turn served as a template for the porous MPs (Figure 1.3h). The porosity and the pore size could be controlled independently by regulating the flow rates of the two immiscible phases. Further, they showed that the overall size of microbeads could be precisely controlled in a wide range by using electrodripping with a pulsed EF applied to the exit needle of the microfluidic device. By using short EF pulses with adjustable amplitude and frequency, they were able to avoid electrocoalescence of the inner droplet phase and further fine-tune the double-emulsion drop sizes. Because of its high reproducibility, high flexibility in terms of achievable particle morphologies, and potential versatility in terms of processable biomaterials, this coupled method advanced the current state of the art of porous MP synthesis.

Recently, Wang et al. generated porous MP adsorbents encapsulated with spongy graphene oxide (GO) by a coaxial capillary microfluidic device composed of inner, middle, and outer capillaries (Figure 1.3i) [84]. The GO solution, silica NPs dispersed in ethoxylated trimethylolpropane triacrylate (ETPTA), and an aqueous surfactant solution were used as the inner, middle, and outer phases, respectively, and were forced to flow through the corresponding capillaries. When these fluids flowed through the capillaries, GO aqueous core droplets were generated at the end of the inner capillary and subsequently encapsulated by a shell drop of the ETPTA at the end of the middle capillary in dripping mode. The overall size and the numbers of the encapsulated core droplets of the double emulsions could be adjusted by tuning the orifice size of the capillaries and the velocities of the three phases. Under UV illumination, the openings of the encapsulated cores to the particle surface were formed because of mechanical damages to the ultrathin and fragile shell layers during the treatment. Such porous spongy structure, together with the encapsulated GO, imparted the MPs with the ability of adsorbing oils both floating on and under water.

1.2.5 Other MMs

MMs with other shapes also show unique properties and have specific applications [89, 90]. For example, cylindrical MMs self-assembled from copolymers can

persist in the blood circulation of rodents 10 times longer than their spherical counterparts. Helical MMs can convert rotational motion into translational motion in liquid media under remote control of a rotated magnetic field, showing great potentials for many applications [91]. Thus, creation of uniform MMs with versatile shapes is crucial for achieving advanced functions. With excellent manipulation of microflows, droplet microfluidics provides a powerful platform for fabricating MMs with versatile structures and compositions. One of the most convenient approaches is to exert spatial confinement. Xu et al. described a versatile strategy of synthesizing tripropyleneglycol diacrylate (TPGDA) MMs in various shapes such as spheres, disks, and rods, by controlling the droplet diameter and cross-sectional geometry (height and width, h and w, respectively) of the microfluidic channel [92]. As shown in Figure 1.4A, when both of the geometries were smaller than ds, the droplet maintained its original spherical shape, when $w > \text{ds}$ and $h < \text{ds}$, that is, the droplet flowed into a wide channel, it changed to a disk shape, and when both of the geometries were smaller than ds, the droplet was confined into a rod-like shape. By illumination with UV light, these droplets were polymerized into solid particles and their shapes were retained. Another facile approach was introduced by Wang et al.; they encapsulated monodisperse droplets generated from microfluidics into cross-linked polymeric networks via interfacial cross-linking reaction in microchannel to produce droplet-containing fiber-like matrices [93]. By stretching and twining the dried fiber-like matrices, the encapsulated droplets could be engineered into versatile shapes from tablet to helix. Based on these deformed droplet templates, versatile MMs were synthesized, such as tablet-like, rod-like, needle-like MMs and complex 3D helices for magnetic-driven rotational and translational motion (Figure 1.4B).

The material shape can also be tailored by controlling the reaction parameters during the solidification process. For example, Lin et al. synthesized tail-shaped alginate MPs in a slow cross-linking process. As shown in Figure 1.4C, sodium alginate droplets were first generated in a microfluidic device and then fell from the oil carrier phase into a $CaCl_2$ solution under gravity [94]. During the slow sedimentation process, the droplets were deformed under the competitive effects of viscous deformation and the interfacial restoring forces, which resulted in the generation of alginate MPs with teardrop or tail shapes. By changing the alginate viscosity and the Ca^{2+} concentration, the size and the morphology of the particles could be tuned. In another interesting study, acorn-like or sharp-edged MMs were fabricated by tuning the wettability properties between two immiscible drops. When the drop pairs were emulsified together in a third carrier fluid phase and came into contact, an equilibrium structure formed in accordance with the spreading coefficient values and droplet volumes. By carefully controlling the interfacial tensions between the two fluid phases using surfactants, the spreading coefficients could be adjusted so that partial engulfment between the two dispersed phases occurred in compliance with the minimum total interfacial energy. Therefore, the drop pairs could finally form a dumbbell- or acorn-shaped configuration. Additionally, Nisisako and Torii synthesized particles with sharp edges by selective polymerization of one of the droplet pairs. They constructed a triphase microfluidic system composed of photocurable monomer 1,6-hexanediol diacrylate (HDDA), a silicone oil phase, and an aqueous phase [95]. Biphasic droplets were generated downstream

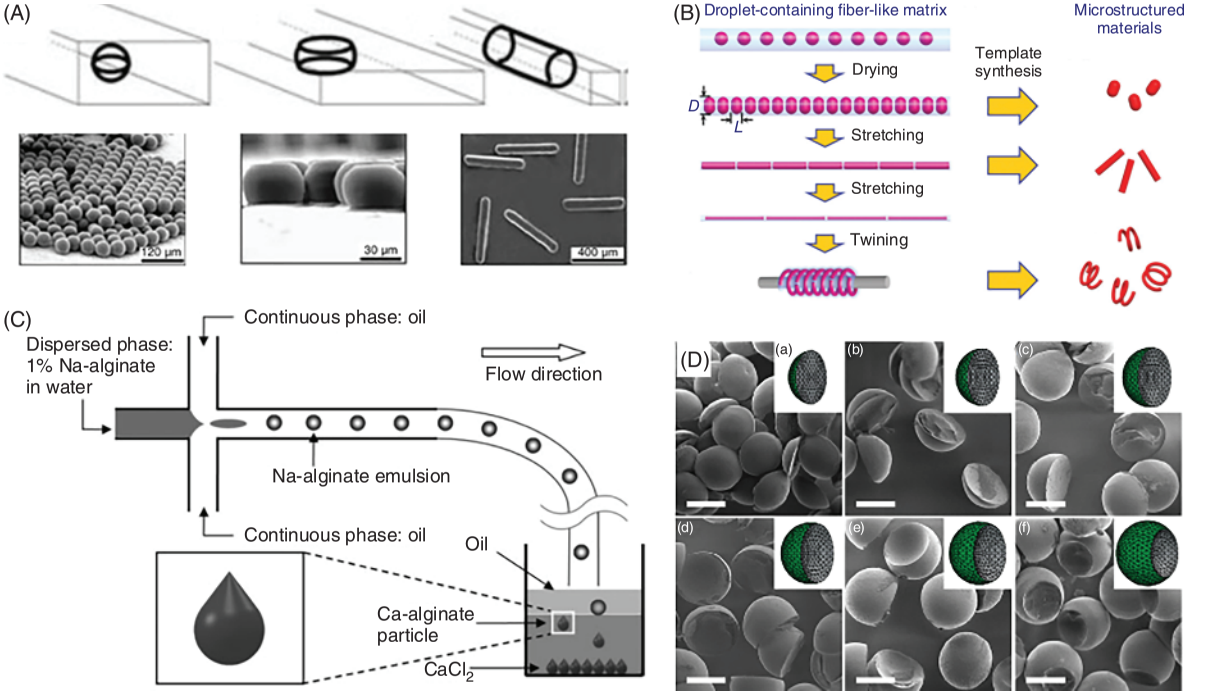

Figure 1.4 (A) Representations of the shapes of droplets in the microfluidic channel, and optical microscopy images of microfluidic MMs based on these deformed droplets. Source: Adapted with permission from Xu et al. [92]. Copyright 2005, John Wiley & Sons. (B) Manipulation of the encapsulated droplets by drying, stretching, stretching, and twining for flexible deformation and synthesis of nonspherical MMs and helices from the deformed droplets. Source: Adapted with permission from Wang et al. [93]. Copyright 2017, John Wiley & Sons. (C) Formation of a tail-shaped Ca-alginate particle from a spherical Na-alginate droplet. Source: Adapted with permission from Lin et al. [94]. Copyright 2013, John Wiley & Sons. (D) MMs of various shapes engineered from Janus droplets containing different volume ratios of silicone oil and the monomer. The scale bars represent 100 μm. Source: Adapted with permission from Nisisako and Torii [95]. Copyright 2007, John Wiley & Sons.

at equilibrium, and MPs were synthesized by photopolymerization of the monomer. It was demonstrated that, with increasing fraction of the HDDA monomer, the particle shape varied from convex to planar and further became concave (Figure 1.4D).

1.3 NMs from Droplet Microfluidics

In recent decades, NMs have drawn significant attention in various applications [96, 97]. Because of electric confinement and surface asymmetry effects, NMs show distinct properties such as optical emission in semiconductor NMs and surface plasmon resonance in noble metal NMs. Additionally, as their dimension is similar to that of biomolecules, they can be tailored to coordinate with biological systems and showed unique properties in imaging, optoelectronics, catalysis, sensing, and drug delivery [98, 99]. The synthesis of NMs goes through four steps: supersaturation, nucleation, growth, and aggregation, and there have emerged many techniques for NM synthesis, which can be classified into two main categories: "top-down" and "bottom-up." [100] Although the properties of NMs are highly related to their size and morphology, it is technically challenging in conventional batch processes to reproducibly fabricate NMs having a desired morphology with a small standard deviation [101].

Since 1990s, much research effort has been devoted to the synthesis of NMs by droplet microfluidics. In contrast to conventional batch systems, the microfluidic method stands out for its intrinsic advantages, including miniaturization, enhanced mass and heat transfer, and reduced time and reagent consumption. Especially, the droplet reactor offers additional fascinating strengths. For example, as the reaction is confined in the microscale droplets, toxic or volatile chemicals can be utilized, and the resultant NMs would not contact the channel walls, thus avoiding possible contamination and blocking. In addition, the advection flow field within the droplets further improves the mixing efficiency, thus offering a well-defined starting point and a consistent residence time, which contributes to a narrower size distribution of the final NMs. Moreover, local control over the synthetic environments could be exerted on separate droplet reactors. Therefore, the reaction parameters scale up linearly, enabling homogeneous synthesis and quantity production [102–105]. Here, we reviewed recent developments in synthesizing inorganic, organic, and other composite NMs through droplet microfluidics.

1.3.1 Inorganic NMs

Inorganic NMs can be classified as amorphous and crystalline ones. Their chemical and physical properties are related to the size, shape, and structure of the particles. Thus, the monodispersity of inorganic NMs should be considered during the formation process, which is largely dependent on the specially controlled reaction kinetics, rapid mixing of the injected precursors, and well-defined time–temperature profiles [106, 107]. All of these parameters

can be precisely regulated in microfluidics based on microscale characteristics [108, 109]. Controllable synthesis of colloidal semiconductor, metal, metal oxide, and hybrid NMs has been demonstrated. For example, Lazarus et al. used a two-phase microfluidic droplet device to synthesize AuNPs and silver nanoparticles (AgNPs) [110]. As shown in Figure 1.5a, a carrier oil phase was injected through inlet 1. The two reaction reagents of a metal salt precursor and the reductant flowed via inlets 2 and 4, respectively. Also, an ionic liquid stream flowed through inlet 3 and served as a stabilizer and also prevented contact of the reaction reagents before droplet formation. When droplets were generated in the T-junction and kept in the dripping regime, the recirculating streamline induced a convective flow, which largely accelerated mixing of the two reaction reagents. This promoted a rapid nucleation burst and thus ensured a homogeneous synthesis environment. As demonstrated by the authors in Figure 1.5b,c, well-dispersed spherical NPs were obtained that were smaller and more monodisperse than those produced in analogous batch reactions as a result of the rapid mixing and the homogeneous reaction environment afforded by the discrete droplets within an immiscible carrier phase.

Besides the demands for homogeneity in NMs, controllable nanostructures are another significant consideration. Based on the flexible design of microfluidic chips and flows, various complex nanostructures have been achieved, such as core–shell NPs, nanogels with controlled pore size, Janus NPs, and other complex materials [100–102]. Shestopalov et al. reported a plug-based, microfluidic method for performing multistep chemical reactions to synthesize CdS/CdSe core–shell NPs with millisecond time control [111]. In this microfluidic method, the investigators first generated droplets from the initial reaction mixture. Two aqueous reagent streams were brought together into the channel where they were allowed to flow laminar alongside each other (labeled R1 and R2 in Figure 1.5d). These reagent streams were then sheared into droplets by an inert stream (labeled S in Figure 1.5d). The winding channels induced mixing by chaotic advection, and the droplets were allowed to react rapidly. To initiate the second stage of the multistep reaction, an aqueous stream of an additional reagent (labeled R3 in Figure 1.5d) was directly injected into the droplets at a junction. The second reaction proceeded as droplets flowed through another length of serpentine channel (Figure 1.5e). Therefore, by conducting multistep reactions in droplets, the CdS/CdSe core–shell NPs were produced and prevented from aggregating on the walls of the microchannels.

Because of the small dimensions of droplets and the closed environment of a pressure-driven flow system, it is typically difficult to control the delivery of chemicals across the continuous phase into the microdroplets. As a result, most applications involve only an initial mixing of all the chemicals prior to the generation of microdroplets. However, many chemical reaction systems require addition of chemicals into generated microdroplets at precise time intervals [113, 114]. An effective method is to directly inject chemicals into the droplets through a side channel, where the chemical solution forms a pendant drop at the junction and merges with the microdroplets passing by. Based on previous studies, Gu et al. presented a novel method that could control material transport into the microfluidic droplets [112]. Instead of using an inert oil as the carrier fluid,

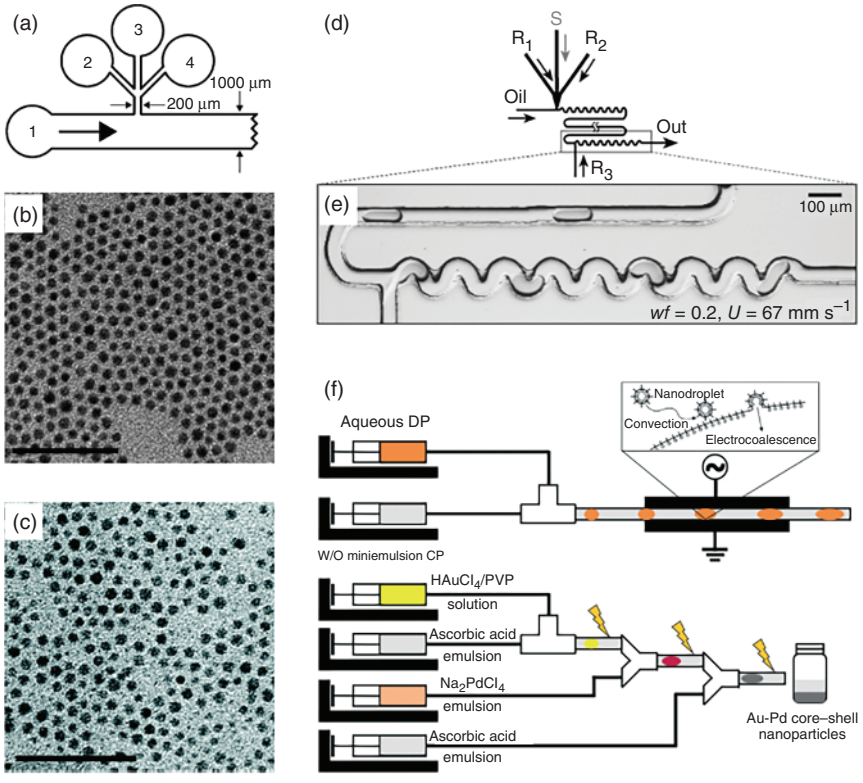

Figure 1.5 (a–c) Schematic representation of the multiple inlet T-junction microfluidic device used to synthesize AuNPs and AgNPs (a); transmission electron microscopy micrographs of AuNPs (b) and AgNPs (c) produced in a droplet-based microfluidic device. Scale bars were 50 nm. Source: Adapted with permission from Lazarus et al. [110]. Copyright 2012, American Chemical Society. (d, e) A schematic diagram of the microfluidic network (d) and a micrograph showing droplets merging with the aqueous stream (e). Source: Adapted with permission from Shestopalov et al. [111]. Copyright 2004, Royal Society of Chemistry. (f) Experimental setup for generating aqueous microdroplets and Au-Pd core–shell NPs with a W/O miniemulsion and electrocoalescence. Source: Gu et al. 2018 [112]. https://pubs.rsc.org/en/content/articlelanding/2018/lc/c8lc00114f#!divAbstract. Licensed under CCBY 3.0.

a W/O miniemulsion was used by the investigators as the continuous phase to generate aqueous monodisperse microdroplets as dispersed phase (Figure 1.5f). The W/O miniemulsion was a thermodynamically metastable system, composed of 50–500 nm aqueous nanodroplets dispersed in an immiscible organic solvent with a stabilizing surfactant. Via electrocoalescence, these nanodroplets served as carriers for chemicals and were transported into the microdroplets. As the nanodroplets were 3 orders of magnitude smaller than the microdroplets, the investigators could easily achieve a nanodroplet-to-microdroplet population ratio of greater than 1 million. Such a large population ratio made it possible to control the chemical addition rate over a wide range, and the addition was in fact "quasi-continuous." Finally, this method was successfully applied to a single-step

synthesis of AuNPs and a multistep flow synthesis of Au-Pd core–shell NPs with a narrow size distribution.

1.3.2 Organic NMs

Amphiphilic molecules such as block copolymers and lipids can self-assemble into NPs when they experience a change in solvent quality. A common and flexible way to accomplish such a change is by mixing the solvent with the antisolvent, where the mixing time directly influences the final size and size distribution of the resultant NPs [115, 116]. However, the heterogeneous environment prevents stabilization of the nascent NPs, facilitates their aggregation, and leads to formation of larger and polydisperse products. In microfluidic systems, the highly efficient mixing of the flow has resulted in polymeric and lipid NPs with tunable size, narrow distribution, and batch-to-batch reproducibility [117, 118]. For example, Hung et al. presented droplet microfluidics-based solvent evaporation and extraction process to enable the controlled generation of monodisperse PLGA particles (Figure 1.6a,b) [119]. A mixture of PLGA-DMSO and water droplets was formed in a carrier phase of silicon oil. After droplet coalescence, DMSO was extracted out into water, and the PLGA nanospheres precipitated as a result of supersaturation. By tuning the PLGA concentration in solvent and the relative flow rates of oil and aqueous phases in the system, they were able to synthesize particles ranging from 70 nm to 30 μm in diameter.

Although the size-controlled synthesis of polymeric NPs was achieved by the aforementioned one-stage microfluidic chips, it is still difficult to synthesize the hybrid core–shell NPs with tunable sizes because of their complex structures. Recently, via a specifically designed two-stage microfluidic chip, Zhang et al. realized the synthesis of controllable core–shell NPs with polymer cores and lipid shells. The first stage of the chip consisted of three inlets and one straight synthesis channel, whereas the second stage had one middle inlet and a spiral synthesis channel (Figure 1.6c) [104]. In mode A, they introduced PLGA solution into the first stage of chip to precipitate intermediate PLGA NPs and injected lipid solution into the second stage to assemble lipid monolayer shell onto the surface of PLGA NPs by hydrophobic attraction between lipid tail and PLGA. In mode B, they generated an intermediate liposome by injecting lipid solution into the first stage, which could reassemble onto the PLGA NPs when PLGA solution was injected into the second stage. In mode A, the NPs were covered by lipid–monolayer–shell, whereas in mode B, NPs were coated by lipid–bilayer–shell. The results indicated an enhanced mixing effect at the high flow rate in microfluidic chips, thus resulting in the assembly of small and monodisperse hybrid NPs.

1.3.3 Other NMs

Metal–organic frameworks (MOFs) are porous crystalline materials consisting of metal clusters or ions that act as connecting nodes and rigid organic bridging ligands. They have attracted immense attention because of their potential for extremely diverse structural topologies and tunable chemical

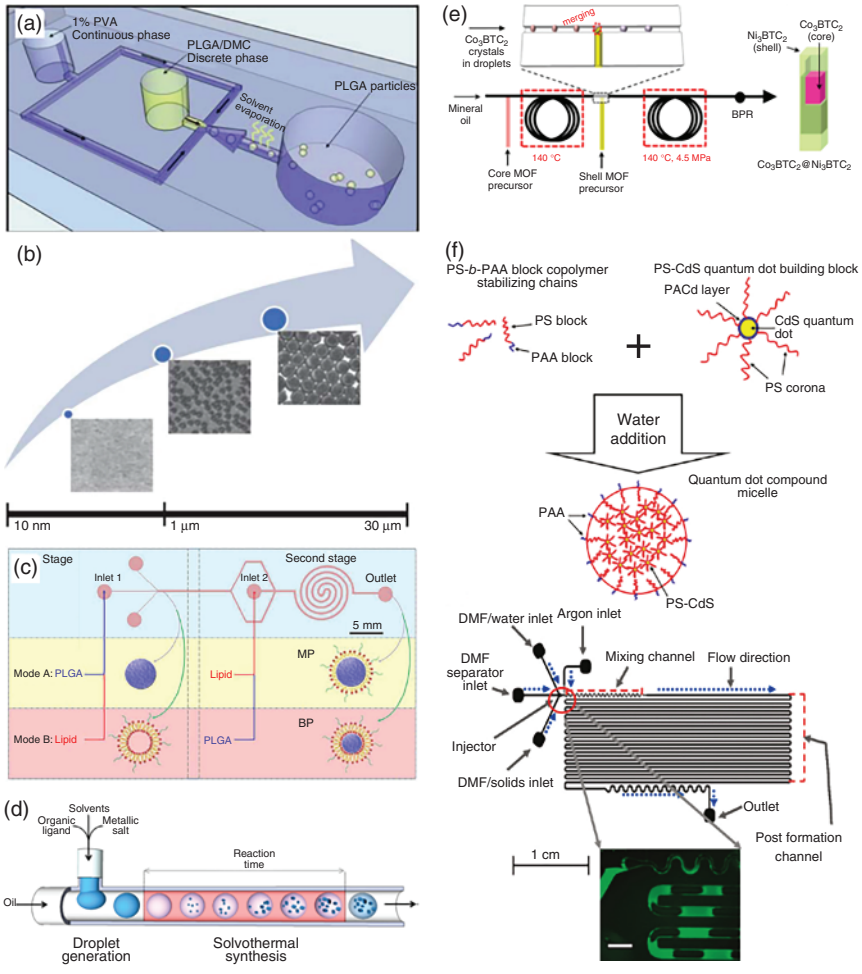

Figure 1.6 (a, b) Schematic of device design for the solvent evaporation method (a) and size graph showing that a wide range of particle sizes were achieved with the extraction and evaporation methods (b). Source: Adapted with permission from Hung et al. [119]. Copyright 2010, Royal Society of Chemistry. (c) Schematic of the two-stage microfluidic chip and generated monolayer-covered or bilayer-covered PLGA NPs. Source: Adapted with permission from Zhang et al. [104]. Copyright 2015, American Chemical Society. (d, e) Schematic representation of the general microchemical process (d) and the integrated hydrothermal microchemical process for synthesis of core–shell MOFs (e). Source: Adapted with permission from Faustini et al. [120]. Copyright 2013, American Chemical Society. (f) Schematic of the QDCM assembly process and the microfluidic reactor. Source: Adapted with permission from Wang et al. [121]. Copyright 2010, American Chemical Society.

functionalities [122, 123]. Microfluidics has recently been employed for the synthesis of MOFs. For example, Faustini et al. reported an ultrafast and continuous synthesis of versatile MOFs with unique morphologies based on microfluidic strategy. Compared to conventional batch processes, the reaction kinetics of MOFs preparation were tremendously improved in confined droplets

(Figure 1.6d) [120]. Representative MOF structures, such as HKUST-1, MOF-5, IRMOF-3, and UiO-66, were synthesized within a few minutes. In addition, three different types of core–shell MOFs composites, i.e. Co_3BTC_2@Ni_3BTC_2, MOF-5@diCH_3-MOF-5, and Fe_3O_4@ZIF-8, were synthesized by exploiting a unique two-step integrated microfluidic system (Figure 1.6e). Unique features such as anisotropic crystal growth or enhanced stability against moisture were observed in these MOFs. Therefore, the microfluidic strategy allowed continuous fabrication of high-quality MOFs crystals and composites exhibiting distinct morphological characteristics in a time-efficient manner.

The droplet platform also provides a microchamber for NM assembly into high-order structures, which exhibit distinct features and potential application values. Wang et al. used a two-phase gas–liquid-segmented microfluidic reactor to control the self-assembly of polystyrene-coated quantum dots (PS-CdS) and stabilizing PS-*b*-PAA block copolymer into quantum dot compound micelles (QDCMs) (Figure 1.6f) [121]. Mixing of water with polymeric constituents was greatly enhanced because of chaotic advection in the liquid plugs as they traveled through the sinusoidal channel. In addition, circulating flow within the liquid plugs provided two convenient handles for size control following initial self-assembly: shear-induced particle breakup and collision-induced particle coalescence. The resulting particle size was a balance of the relative rates of these fluids under a specific set of experimental parameters. By changing the self-assembly conditions, the mean particle size was tuned in the range of 40–137 nm. These results demonstrate that microfluidic strategies have obvious advantages in controlling self-assembly of block copolymers and other colloids.

1.4 Applications of the Droplet-Derived Materials

Droplet microfluidics enables synthesis of materials with uniform and highly controlled sizes and structures. By incorporating specific ingredients, such materials could be endowed with distinct physical and chemical properties such as optical features, mechanical strength, selective permeability, and stimulus-responsive capacity. Therefore, they are highly applied in various fields. Herein, we categorize their applications into several aspects.

1.4.1 Drug Delivery

Encapsulation and controlled release of active agents are of significant interest in developing advanced delivery system for drugs, nutrients, fragrances, and cosmetics. Especially, for efficient drug delivery, the agents should be encapsulated within carriers with desired doses and then released in a specific target location [124, 125]. However, the clinical translation of drug delivery systems is relatively slow, which can be partially ascribed to the poor control of the preparation processes in the conventional batch method [126]. For example, the polymeric particles prepared by the conventional batch method usually show high batch-to-batch variations in physicochemical properties, such as the average

particle size, size distribution, surface charge, and drug release profiles. Materials synthesized by droplet microfluidics possess several advantages to overcome the dilemma, which lie in the following aspects. First, droplet-synthesized materials are highly tunable and uniform in size, structure, and encapsulation efficiency. This provides a guarantee for maintaining a consistent release response and thus for regulating the release rate. Second, the droplet-based drug delivery system allows for a wide range of material choices, and multiple drugs could be loaded simultaneously for investigating their synergetic effects. Third, by using different matrix materials, various release profiles can be achieved under an external stimulus, which are important for specific usages [127, 128].

Many MP-based drug delivery platforms are developed through O/W single emulsion, where the drugs are encapsulated into a biocompatible polymeric particle matrix, including PLGA, poly-ϵ-caprolactone, and hydroxypropyl methylcellulose acetate succinate (HPMCAS). The polymers used in O/W emulsions are typically dissolved in a volatile solvent that can evaporate or diffuse out from the droplets. The size of MPs is primarily controlled by the droplet size and how much the final droplet shrinks during solvent removal, an adjustable variable by employing different polymer concentrations [124]. For example, Xu et al. fabricated monodisperse biodegradable drug-loaded PLGA MPs by combining the formation of droplets in a microfluidic flow-focusing generator with rapid evaporation of solvent from the droplets (Figure 1.7a,b) [129]. By comparison, they demonstrated that microfluidics-based, monodisperse MPs exhibited significantly reduced burst release and slower release rates than conventional, polydisperse MPs of similar average sizes and overall loading of drug. Therefore, the ability of droplet microfluidics to produce monodisperse particles for drug delivery has several practical advantages. In addition, the reduced shear stresses used to prepare particles in a microfluidic device may assist in maintaining the bioactivity of shear-sensitive biomolecular drugs. Given that the conventional emulsion approach typically produces aggregates that must be removed by filtration, particles prepared using the microfluidic method can be produced with higher yields, which is also a significant advantage particularly for expensive drugs.

Single emulsions do not ensure the simultaneous loading of multiple therapeutics, especially when the payloads present different solubility. Therefore, double emulsions are also widely used in drug delivery applications. Li et al. presented a new type of MPs with gelatin methacrylate (GelMa) cores and PLGA shells for synergistic and sustained drug delivery applications (Figure 1.7c) [130]. The MPs were fabricated by using GelMa aqueous solution and PLGA oil solution as the raw materials of the microfluidic double-emulsion templates, in which hydrophilic and hydrophobic actives, such as doxorubicin hydrochloride (DOX, hydrophilic) and camptothecin (CPT, hydrophobic), could be loaded, respectively. As the inner cores were polymerized in the microfluidics during the formation of the double emulsion, the solute actives could be trapped in the cores with high efficiency, and the rupture or fusion of the cores could be avoided during the solidification of the MP shells with other actives. It was also demonstrated that the core–shell MPs with DOX and CPT codelivery could significantly reduce the viability of liver cancer cells. These features made the solid core–shell MPs ideal for synergistic and sustained drug delivery applications.

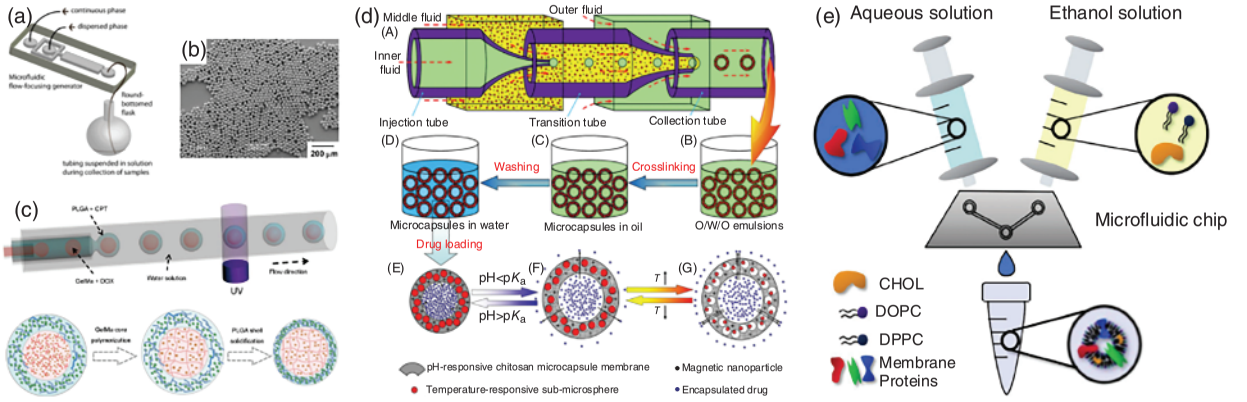

Figure 1.7 (a, b) Schematic illustration of the procedure to fabricate monodisperse polymer MPs (a), and scanning electron microscopy images of monodisperse PLGA MPs with a narrow size distribution (b). Source: Adapted with permission from Xu et al. [129]. Copyright 2009, John Wiley & Sons. (c) Schematic diagram of a capillary microfluidic system for generating the W/O/W double-emulsion templates with polymerized cores and the fabrication process of the drug-loaded GelMa–PLGA core–shell MPs. Source: Adapted with permission from Li et al. [130]. Copyright 2017, Springer Nature. (d) Schematic illustration of fabrication process and controlled release mechanism of the proposed multi-stimuli-responsive microcapsules. Source: Adapted with permission from Wei et al. [131]. Copyright 2014, John Wiley & Sons. (e) Schematic process for the assembly of biomimetic nanovesicles using NanoAssemblr platform. Source: Adapted with permission from Molinaro et al. [132]. Copyright 2018, John Wiley & Sons. (f) Schematic of the two-stage microfluidic chip for synthesizing the lipid-PLGA hybrid NPs. Source: Adapted with permission from Feng et al. [133]. Copyright 2015, American Institute of Physics. (g) High-resolution scanning electron microscopy images of TOPSi NPs, TOPSi@AcDEX nanosystems, and TOPSi@AcDEX@CCM nanovaccines. Source: Adapted with permission from Fontana et al. [134]. Copyright 2017, John Wiley & Sons.

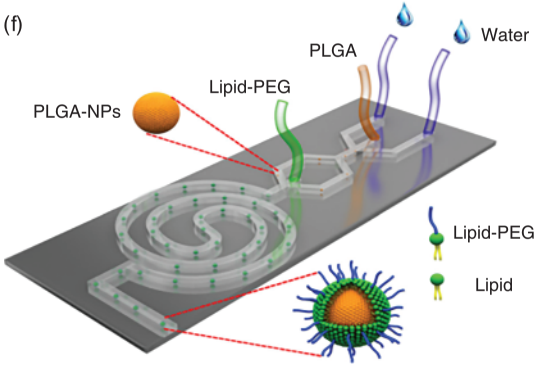

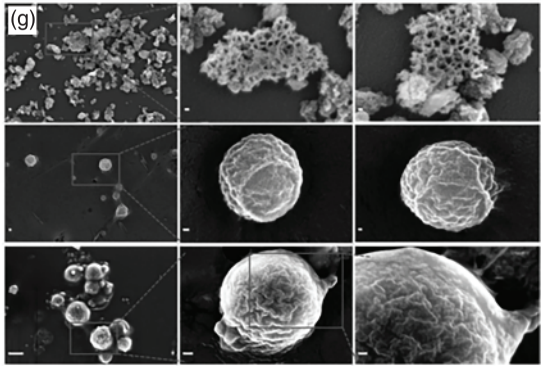

Figure 1.7 (*Continued*)

In passive modes, drug release depends on molecular diffusion and matrix degradation, and the release profile generally shows an initial burst step and a following sustained pattern. MPs with multi-stimuli-responsive properties have been prepared by droplet microfluidics to achieve enhanced control over drug release. For instance, based on W/O/W emulsions, Wei et al. fabricated microcapsules composed of cross-linked chitosan acting as a pH-responsive capsule membrane (Figure 1.7d) [131]. When the local pH was lower than the pK_a of chitosan, the membrane swelled, resulting in a high drug release rate. The release rate could be further tuned by varying the interspace distance between the nanosphere in the capsule membrane, which was achieved by the temperature-regulated volume change of the nanospheres. In addition, the magnetic NPs were embedded to realize "site-specific targeting," and the temperature-responsive submicrospheres were embedded to serve as "microvalves." Therefore, this kind of multi-stimuli-responsive MPs provided a new direction for designing "intelligent" controlled release systems and expected to realize more rational drug administration.

NMs with unique physical and chemical properties can also serve as drug carriers. In addition, more recently, advances in biomimicry, i.e. the biologically inspired design of materials, has spurred the development of novel strategies to bestow NMs with multiple functionalities necessary to negotiate biological barriers. Current approaches for drug delivery carriers include mimicking of leukocytes, red blood cell platelets, and cancer cells to achieve superior delivery of therapeutics compared to conventional NMs. These biomimetic strategies demonstrated innate biological features and intrinsic functionalities typical of the donor cell source. For example, leukocyte-like nanovesicles showed prolonged circulation and preferential targeting of inflamed vasculature, while platelet-like NPs displayed platelet-mimicking properties such as adhesion to damaged vasculature and binding to platelet-adhering pathogens. Molinaro et al. successfully applied the microfluidics-based NanoAssemblr platform for the incorporation of membrane proteins within the bilayer of biomimetic nanovesicles (leukosomes) (Figure 1.7e) [132]. The physical, pharmaceutical, and biological properties of microfluidics-formulated leukosomes (called NA-Leuko) were characterized, which showed extended shelf life and retention of the biological functions of donor cells (i.e. macrophage avoidance and targeting of inflamed vasculature). Thus, the microfluidic approach represents as a universal, versatile, robust, and scalable tool, which is extensively used for the manufacturing of biomimetic nanovesicles.

Core–shell NPs have gained increasing interest for drug delivery because of their high flexibility and biocompatibility. However, it is too complex and laborious to synthesize controlled core–shell NPs in bulk approaches. Microfluidic systems integrated with the precise flow control and hydrodynamic flow focusing have been applied to fabricate size-tunable lipid–polymer NPs. Jiang's group designed a two-stage, high-throughput microfluidic chip to fabricate monodisperse lipid–polymer NPs with a controlled size (Figure 1.7f) [133]. The core of the NPs was a PLGA polymer and the shell consisted of dipalmitoyl phosphatidylcholine (DPPC), 1,2-distearoyl-*sn*-glycero-3-phosphoethanolamine-*N*-poly(ethylene glycol) (DSPE-PEG), and cholesterol. It showed that the higher the flow rate, the better the mixing performance was, which led to smaller sized

NPs in the microfluidic platform. *In vitro* experiments showed that the large hybrid NPs more likely to be aggregated in serum and exhibit a lower cellular uptake efficacy than the smaller ones. In another example, Fontana et al. adopted the glass capillary microfluidic nanoprecipitation technique to produce the core–shell NPs. Thermally oxidized porous silicon (TOPSi) NPs were encapsulated into acetalated dextran (AcDEX) or spermine-modified acetalated dextran (SpAcDEX) polymeric particles. The particles coated with AcDEX were then co-extruded together with vesicles derived from cancer cell membrane (CCM) to obtain the final core–shell system (TOPSi@AcDEX@CCM) (Figure 1.7g) [134]. TOPSi@SpAcDEX particles were functionalized with a model antigen, Trp2, to provide the second system (TOPSi@SpAcDEX-Trp2). They employed this model antigen to evaluate the ability of the system to work as an adjuvant. The adjuvant NPs presented high monodispersity because of the efficient mixing produced in the microfluidic device and were shown to be highly cytocompatible. In addition, the NPs induced the expression of costimulatory signals both in the immortal cell lines and in peripheral blood monocytes. TOPSi@AcDEX@CCM greatly enhanced the secretion of IFN-γ in peripheral blood monocytes and did not induce the secretion of IL-4, thereby orienting the polarization of the newly primed T-cells toward a Th1 cell-mediated response. Therefore, the developed nanovaccines showed promising adjuvant properties and the possibility of encapsulating the nanosystems with materials derived from the patient's tumor opened new prospects in the field of personalized cancer medicine.

1.4.2 Cell Microencapsulation

Cell microencapsulation is a decade-old concept with many applications, such as cell therapy, cell biosensors, cell immobilization for antibody production, and probiotic encapsulation by the food industry [135, 136]. *In vitro* recapitulation of the 3D microenvironment that cells face in the human body has emerged as a powerful approach for addressing biomedical challenges such as control of stem cell fate or assessment of drug efficacy. In order to achieve this goal, biochemical and biophysical aspects of the 3D cellular microenvironment are typically imitated. Recently, microfluidics-enabled cell encapsulation has emerged as an interesting strategy to construct hydrogels and establish customized cellular microenvironments. Based on the microfluidic emulsification in which highly monodisperse surfactant-stabilized aqueous microdroplets are formed at the junction of microfluidic channels or in coaxial capillaries, the high-throughput handling of cells could be achieved. In the simplest case, cell-laden microgels can be prepared by encapsulating cells in W/O emulsions, followed by gelation. For example, Kapourani et al. employed biorthogonal, microfluidic templating to produce three different cell-laden polyglycerol-based matrices (Figure 1.8a–c) [137]. Star-shaped polyglycerol hexaazide, α,*ω*-bis azido-linear polyglycerol or polyethylene glycol, as well as dendritic polyglycerol-(polycyclooctyne) served as bioinert hydrogel precursors. Because of the multifunctional nature of the cytocompatible polymeric building blocks and the microfluidic patterning, the authors demonstrated the generation of entirely polyglycerol-based microcapsules with excellent stability and full retention of viability of the packed cells for longer than three weeks.

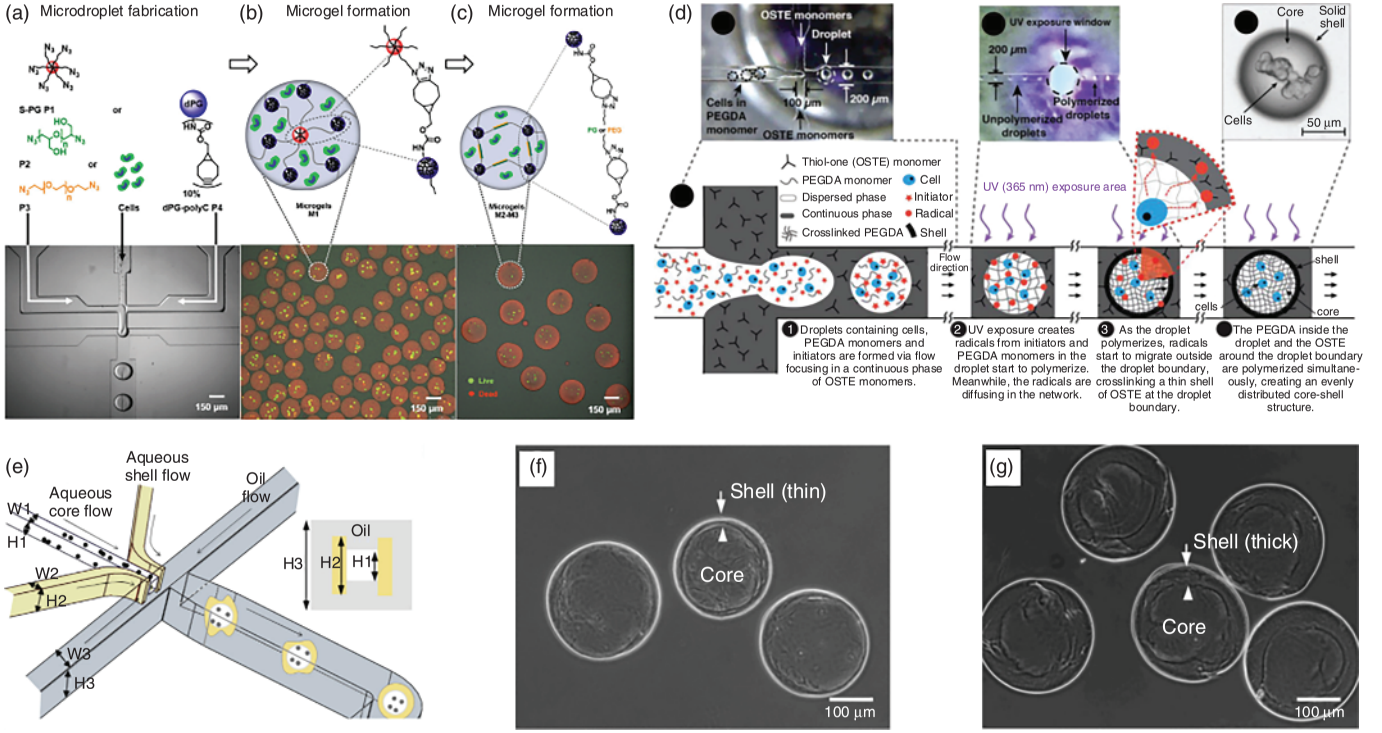

Figure 1.8 (a–c) Droplet-templated cell encapsulation: a set of azide-functionalized precursors and dPG-polyC was prepared (a), cell-laden microgel particles deriving from S-PG-hexaazide (b), and from α,ω-bis-azido-LPG and α,ω-bis-azido-PEG (c), were formed, respectively. Source: Adapted with permission from Kapourani et al. [137]. Copyright 2018, John Wiley & Sons. (d) Illustration of the one-step curing mechanism for core–shell particle synthesis in a droplet microfluidic setup, and microscopy image of the generated gel core–solid shell particle that contains cells. Source: Adapted with permission from Zhou et al. [138]. Copyright 2018, John Wiley & Sons. (e–g) Nonplanar microfluidic flow-focusing device for one-step generation of core–shell microcapsules from two aqueous fluids (e), typical phase contrast images of microcapsules of ~240 μm with a thin (~10 μm) shell (f), and ~260 μm with a thicker (~50 μm) shell (g). Source: Adapted with permission from Agarwal et al. [139]. Copyright 2013, Royal Society of Chemistry

Other than simple spherical particles, microcarriers with complex shapes and microstructures are also designed. Microcapsules templated from W/O/W double emulsions have been generated for cell encapsulation and can be categorized into two types: matrix-core/shell and liquid-core/shell microcapsules. Incorporating cells in the core of the microcapsules enhances their resistance against external effects, such as enzymatic attack and UV irradiation, and prevents them from regressing. For example, Zhou et al. introduced cell encapsulation in core–shell particles with a synthetic polyethylene glycol diacrylate (PEGDA) hydrogel core and a solid off-stoichiometry thiol-ene polymer (OSTE) shell [138]. The MPs were synthesized by using a droplet microfluidic chip with a flow focusing junction to generate droplets that consisted of a dispersed phase of PEGDA monomers, cells, and UV initiator and a continuous phase of OSTE monomers (Figure 1.8d). Core–shell cell encapsulation was achieved after a single UV exposure. The encapsulated human cells in 100 μm diameter particles had >90% viability. The average shell thickness was controlled between 7 and 13 μm by varying the UV exposure, and the shell was measured to be permeable to low-molecular-weight species (<180 Da) but impermeable to higher molecular weight species (>480 Da). The unique material properties and the orthogonal control of the MP core size, shell thickness, shell permeability, and shell surface properties addressed the key unresolved challenges in the field and were expected to promote translation of novel cell therapy concepts from research to clinical practice.

Microcapsules with liquid–core/shell structure allow encapsulated cells to form cell aggregates in the liquid core because of enhanced cell–cell interactions. This strategy is of special value for stem cell studies. For example, the comparison between cells cultured in solid microbeads and liquid–core/shell microcapsules showed that the latter allowed formation of single spherical embryoid body cells within two days. In contrast, cells in the solid microbeads only formed bumpy shapes from several clusters of cells. Agarwal et al. microfabricated a 3D microfluidic flow-focusing device to achieve one-step generation of core–shell microcapsules with an alginate hydrogel shell of controllable thickness and an aqueous liquid core of embryonic stem (ES) cells without using any cytotoxic chemicals or organic solvents (Figure 1.8e) [139]. The core–shell architecture of the microcapsules resembled that of a prehatching embryo where ES cells resided naturally (Figure 1.8f,g). ES cells encapsulated in the liquid core of the microcapsules were found to survive well (>92%) and proliferate to form a single aggregate in each microcapsule within seven days. Furthermore, the aggregated cells were found to have significantly higher expression of pluripotency marker genes compared to the ES cells cultured on 2D substrates and they could be efficiently differentiated into beating cardiomyocytes under the induction of a single small molecule without complex combination of multiple growth factors.

1.4.3 Tissue Engineering

In the past decade, TE has been demonstrated to be increasingly potential for creating true biological alternatives for artificial implants and prostheses for becoming an on-demand regenerative tool alternative to harvested tissue/organ

transplantation. The underlying concept of TE consists of few steps in which healthy cells are first isolated from a patient's biopsy, expanded *in vitro*, and then seeded/encapsulated into a carrier. The resulting engineered construct is often precultured *in vitro* and then grafted back into the patient to regenerate and/or replace the damaged tissue [140, 141]. Tissues are integrated 3D structures of multiple types of cells and ECMs. The function of a tissue is typically governed by multiple cues, such as intercellular signaling and cell interactions with the surrounding ECMs. Cell-laden microgel "modules" carrying different types of cells can be combined or reconfigured to mimic various types of tissues. These microgels generated from microfluidics serve as building blocks for construction of TE scaffolds. Their applications in TE, including organ-on-a-chip, bone/cartilage regeneration, stem cell culture, and therapy, have been extensively studied [142, 143].

The small size of the hydrogel MPs is particularly attractive for injectable cell delivery systems in regenerative medicine, as it allows direct delivery of cells through needles to the damaged tissue area. The direct injection minimizes surgical invasiveness and thus is beneficial in practical clinical applications. Hou et al. developed injectable degradable PVA microgels using a microfluidic approach for encapsulation of mesenchymal stem cells (MSCs) and bone morphogenetic protein-2 (BMP-2), which provided favorable microenvironments for cell proliferation and controlled osteogenic differentiation *in vitro* (Figure 1.9a–c) [144]. PVA microgels formed with various polymer concentrations exhibited different degradation and mechanical properties as well as the release profiles of growth factors. The mild cross-linking conditions and cell-compatible materials facilitated the encapsulation of MSCs with high bioactivity, which ensured prolonged cell survival, proliferation, and migration. Additionally, BMP-2 coencapsulated into the microgel environments enhanced osteogenic differentiation of MSCs. In another separate work, bioactive fibrin microbeads with bioactive molecules were produced using a droplet microfluidic platform. $\alpha_2PI_{1\text{-}8}$-MMP-IGF-1-conjugated microbeads were mixed with genipin-cross-linked collagen, resulting in a novel injectable bulking agent, which promoted human urinary tract smooth muscle cell (hSMC) migration *in vitro* (Figure 1.9d) [145]. This injectable material showed similar rheological characteristics as the reference sample. The regenerative potential of this bioactive bulking agent was evaluated in a rabbit model and might promote functional regeneration of human urinary tract smooth muscle tissue for long-term treatment of stress urinary incontinence.

With the advantages of using microfluidics to fabricate MPs, the dimensions of the microspheres could be precisely controlled to form desirable scaffold structures. However, it was not easy to fabricate ultra-high-porosity scaffolds because the porosity of the scaffolds is determined by the gaps between microspheres after packing. For microspheres with diameters of $\approx$100 μm, the gap was only several micrometers. Hollow microspheres were investigated because they have more adjustable parameters to provide greater flexibility as well as a larger contact surface area to interact with cells. Yu et al. used a droplet-based microfluidic process to fabricate hollow bacterial cellulose (BC) MPs by culturing Gram-negative bacterium *Gluconacetobacter xylinus* (*G. xylinus*) inside

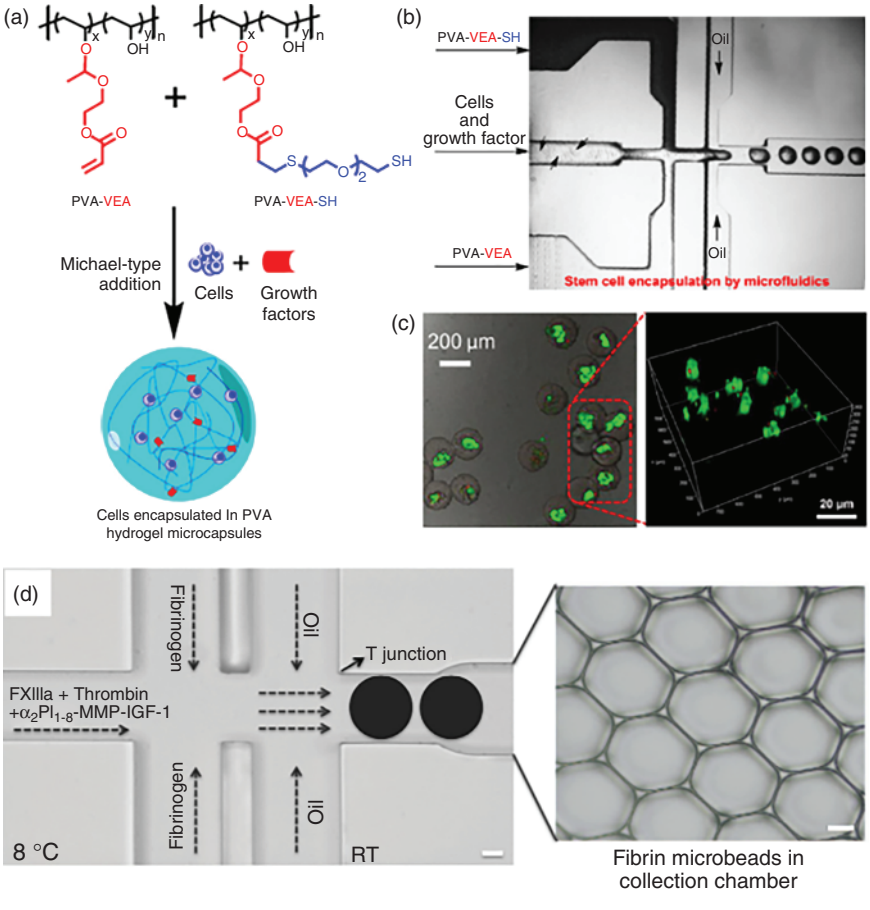

Figure 1.9 (a–c) Schematic illustration of PVA microgels formed by PVA–VEA and PVA–VEA–SH through a Michael-type addition reaction for encapsulation of stem cells and growth factors (a); image of the microfluidic device used for PVA microdroplet formation, the arrows indicated the cells suspending in the culture medium (b); confocal microscopy images of MSCs cultured in PVA microgels, live cells were labeled with calcein AM (green) (c). Source: Adapted with permission from Hou et al. [144]. Copyright 2018, Elsevier. (d) Schematic of microfluidic channels of the microchip used for fibrin microbead fabrication and bright-field microscopy image of the microbeads. Source: Adapted with permission from Vardar et al. [145]. Copyright 2018, Elsevier. (e) The microfluidic process for producing the double-layer alginate core agarose shell microdroplet as cellulose secretion template and the following steps to produce hollow BC microsphere including gelling, cellulose secretion, purification, and the application of the microsphere as a cell culture scaffold *in vitro* and an injectable scaffold for wound healing *in vivo*. Source: Adapted with permission from Yu et al. [146]. Copyright 2016, John Wiley & Sons.

a double-layer hydrogel template [146]. The generated microgels were washed and stored under static culture conditions for the production of cellulose from *G. xylinus*. The cellulose fibers became gradually entangled and confined in the shell part of the particles, which formed the desirable hollow morphology. The template gel was then removed using thermal and chemical treatments

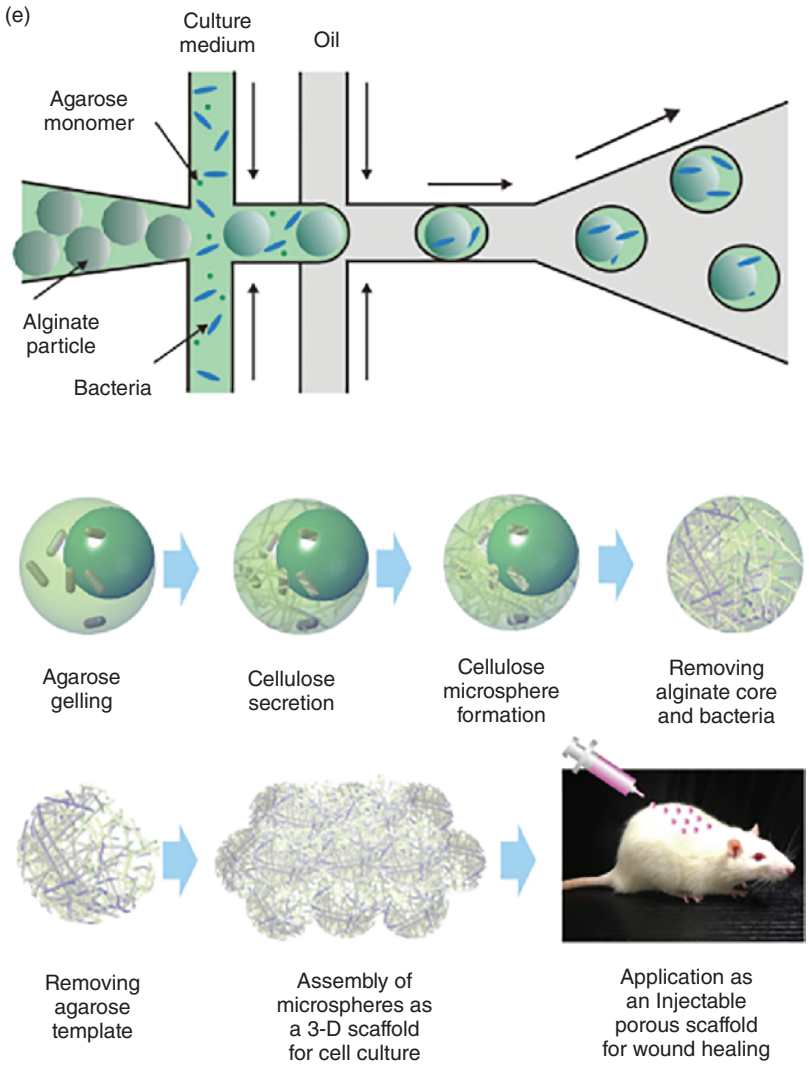

Figure 1.9 (*Continued*)

without affecting the cellulose, thus generating hollow BC microspheres. With the advantage of hollow BC microspheres, scaffolds with high porosity were developed for 3D cell culture and could be used as an injectable scaffold *in vivo* for wound healing (Figure 1.9e).

Currently, droplet microfluidics is mainly based on the W/O system, in which the organic reagents are used as continuous phase. However, the system is limited by the addition of the oil phase and/or surfactants, thus limiting their applications in TE. Liu et al. described a new microfluidic strategy for controllable and high-throughput generation of monodispersed W/W droplets

[147]. Solutions of polyethylene glycol and dextran were used as continuous and dispersed phases, respectively, without any organic reagents or surfactants. The size of W/W droplets could be precisely adjusted by changing the flow rates of dispersed and continuous phases and the valve switch cycle. In addition, uniform cell-laden microgels were fabricated by introducing the alginate component and rat pancreatic islet cell suspension to the dispersed phase. The encapsulated islet cells retained high viability and the function of insulin secretion after cultivation for seven days. The high-throughput droplet microfluidic system with high biocompatibility was stable, controllable, and flexible, which could boost various chemical and biological applications, such as bio-oriented MPs synthesizing, microcarriers fabricating, TE, etc.

1.4.4 Biosensors

Biosensors are devices composed of biological recognition elements and signal transduction elements for quantitative and semiquantitative analysis [148, 149]. An ideal biosensor can detect analytes, such as glucose, enzymes, DNA, and antibodies in a rapid, efficient, and convenient manner. They are increasingly in demand for many biomedical applications from fundamental biological studies to clinical diagnostics. Metal NP-based sensors have been extensively studied. These biosensors are based on the localized surface plasmon resonance (LSPR) phenomenon of metal NPs and is highly associated with the size, shape, dielectric properties, aggregate morphology, surface modification, and refractive index of the surrounding medium [150]. AuNPs and AgNPs are the most common NPs fabricated for LSPR, and the synthesis of other metal NPs such as Pt and copper has also been attempted. Microfluidic synthesis offers fine-tuning and convenience in adding new agents for multistep reactions. For instance, Lohse et al. demonstrated a simple microfluidic reactor constructed from commercial components for generate hydrophilic functionalized AuNPs (Figure 1.10A) [151]. The authors showed that the synthesis of AuNPs in the reactor could be fine-tuned to control the aspect ratios and absolute dimensions. The reactor could also be easily integrated with UV–vis absorbance spectroscopy analysis to monitor in real time and to analyze the purity of AuNPs as quality control.

Binary noble metal NPs have been synthesized for LSPR based on microfluidic system. Knauer et al. generated noble metal NPs with multishell structures with a two-step microreactor (Figure 1.10B) [152]. It was shown that a more uniform particle growth was reached by the use of microfluidic techniques for the synthesis of multishell NPs. The improvement of the particle size distribution corresponded to an enhanced quality of the optical spectra. The absorption spectra of the particle dispersions synthesized in the microflow-based system showed a blue shift combined with a narrower bandwidth, which clearly emerged in the case of Au/Ag/Au core/double-shell particle. As expected, the spectral position of the plasmonic resonance shifted dramatically by covering a gold seed particle with an alternating shell structure of gold and silver. Thus, the position of the resonance peak could be adjusted within a wide range of optical spectra

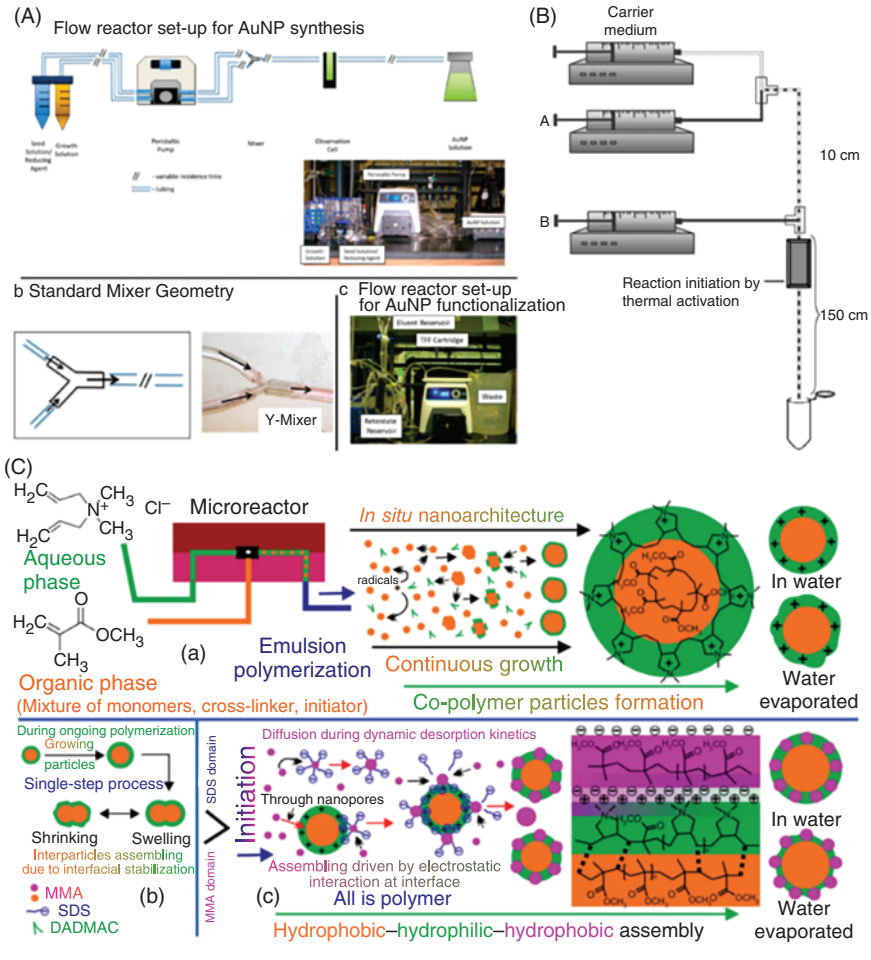

Figure 1.10 (A) The integrated millifluidic reactor used for AuNPs synthesis and functionalization. Source: Adapted with permission from Lohse et al. [151]. Copyright 2013, American Chemical Society. (B) General setup for microsegmented flow synthesis of bimetallic multishell NPs. Source: Adapted with permission from Knauer et al. [152]. Copyright 2011, Elsevier. (C) Schematic overview of *in situ* nanoarchitecture of the copolymer NPs by emulsion polymerization via micro-flowthrough technique, interparticles nanoassembling of polymer particles during ongoing polymerization, and controlled hydrophobic/hydrophilic/hydrophobic electrostatic nanoassembly particles. Source: Adapted with permission from Visaveliya and Köhler [150]. Copyright 2015, John Wiley & Sons. (D) Schematic illustration of the buckling of semipermeable capsules subjected to positive osmotic pressure, and confocal microscopy images of a mixture of four distinct microcapsules dispersed in an aqueous solution of 475 mOsm/l, whereby the red, orange, yellow, and green capsules contain aqueous solutions of 33, 342, 649, and 950 mOsm/l, respectively. Source: Adapted with permission from Kim et al. [153]. Copyright 2014, John Wiley & Sons.

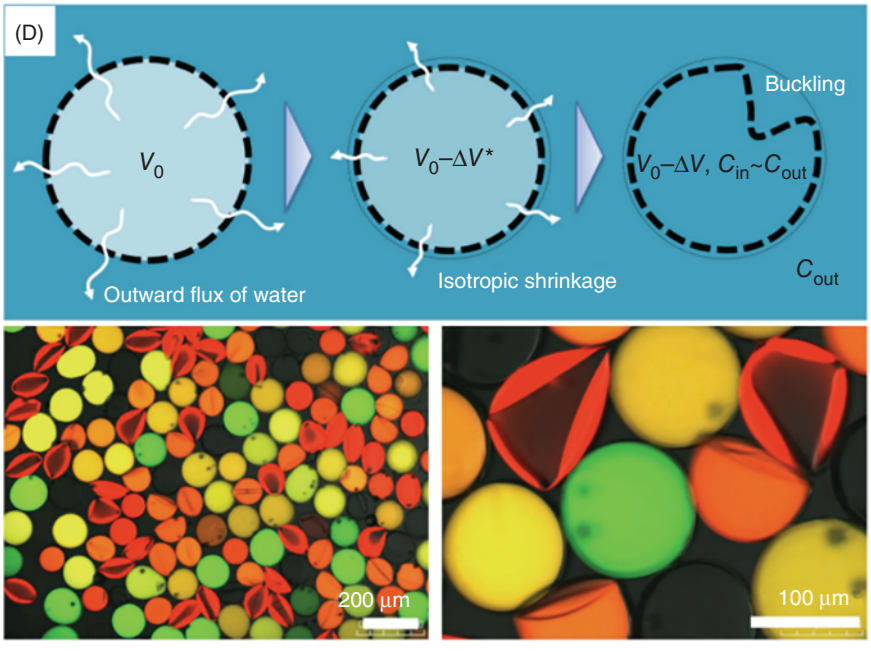

Figure 1.10 (*Continued*)

only by the deposition of a next metal shell. The investigations showed that the micro-continuous-flow synthesis was well suited for the preparation of composite plasmonic NPs. The polymer/metal NPs could also be applied as biosensors. For example, Visaveliya and Köhler presented a semimicrofluidic approach for a single-step *in situ* copolymer interaction to generate core–shell-type PMMApolyDADMAC particles and their assemblies with polymer and metal NPs (Figure 1.10C) [150]. This study revealed that the mean polymer particle size could be tuned between 200 nm and 1 μm at different process conditions regulated by microfluidic platform. Interfacial copolymerization induced the controlled compartmentalization where a hydrophobic core adopted spherical shape in order to minimize the surface energy and simultaneously sheltered in the hydrophilic shell-like surface layer. Surface layer could swell in the aqueous medium and allow controlled entrapping of functional hydrophobic NPs in the hydrophilic interior via electrostatic interaction, which could be particularly interesting for combined fluorescence activity. Furthermore, the polymer–metal nanoassembly particles could be implemented as an ideal surface-enhanced Raman scattering substrate for detection of the trace amounts of various analytes.

Apart from NPs, MPs could also serve as important sensors in response to environmental parameter variations. For example, Kim et al. reported a microfluidic approach to produce microcapsules with ultrathin and semipermeable membranes, providing a facile and direct measurement of the osmotic strength [153]. Using capillary microfluidic devices, W/O/W double-emulsion drops with an ultrathin middle phase were prepared, which transformed into polymeric microcapsules that contain an aqueous solution with standard osmotic strength

upon solidification of the middle phase. The resultant microcapsules are highly sensitive to osmotic pressure differences because of the semipermeability and very small thickness of the membrane. Therefore, a small positive pressure could lead to buckling of the capsules by an outward flux of water through the membrane. Therefore, when a mixture of distinctively labeled microcapsules containing different standard osmotic solutions were dispersed in an unknown solution, the capsules were selectively buckled according to the positive pressure, thereby enabling an estimation of the osmotic strength (Figure 1.10D).

1.4.5 Barcodes

The increasing application of high-throughput assays in biomedical areas, including drug discovery and clinical diagnostics, demands effective strategies for multiplexing [154]. One promising strategy is the use of barcode particles that encode information about their specific compositions and enable simple identification. Microfluidics is an effective approach that has created exciting avenues of scientific research in barcode particle synthesis. The resultant particles have found important applications in the detection of multiple biological species as they have properties of high flexibility, fast reaction times, less reagent consumption, and good repeatability. For example, Gerver et al. used a customized and fully automated microfluidic device to mix different predetermined ratios of nanophosphors suspended in monomer, followed by photopolymerization, resulting in spectrally encoded polymer (Figure 1.11a,b) [155]. Using this method, the authors produced, imaged, and characterized thousands of encoded beads with 24 distinct spectral codes. The beads were highly uniform in size and had a very tight distribution of lanthanide ratios, so that investigators could distinguish between the codes with 0.1% error. These results established the practical feasibility of using lanthanide nanophosphors for spectral encoding and lay the foundation for future high-throughput multiplexing of biological assays.

Quantum dots (QDs) have narrow Gaussian emission line shapes, resistance to photobleaching, high quantum yields, single-wavelength excitation, and a large number of codes. Thus, they are an ideal additive to emulsions for generating barcode particles [158]. Zhao et al. developed a new approach to prepare barcode particles by encapsulating QDs in double-emulsion templates generated in capillary microfluidic devices (Figure 1.11c) [156]. The resultant particles exhibited uniform spectral characteristics and allowed substantial numbers of coding levels for multiplexing (Figure 1.11d). In addition, the approach also enabled fabrication of anisotropic magnetic barcode particles, which could rotate under a rotating magnetic field and aggregate under a stationary magnetic field. This feature created new opportunities to perform magnetic separation of the barcode particles. Therefore, the QD-containing barcode particles were promising as microcarriers in biomedical applications, including high-throughput bioassays and cell culture research where multiplexing was needed.

Photonic crystals (PhCs) are a kind of well-known photonic NMs with spatially ordered lattices that exhibit brilliant structural colors [159]. By constructing PhCs

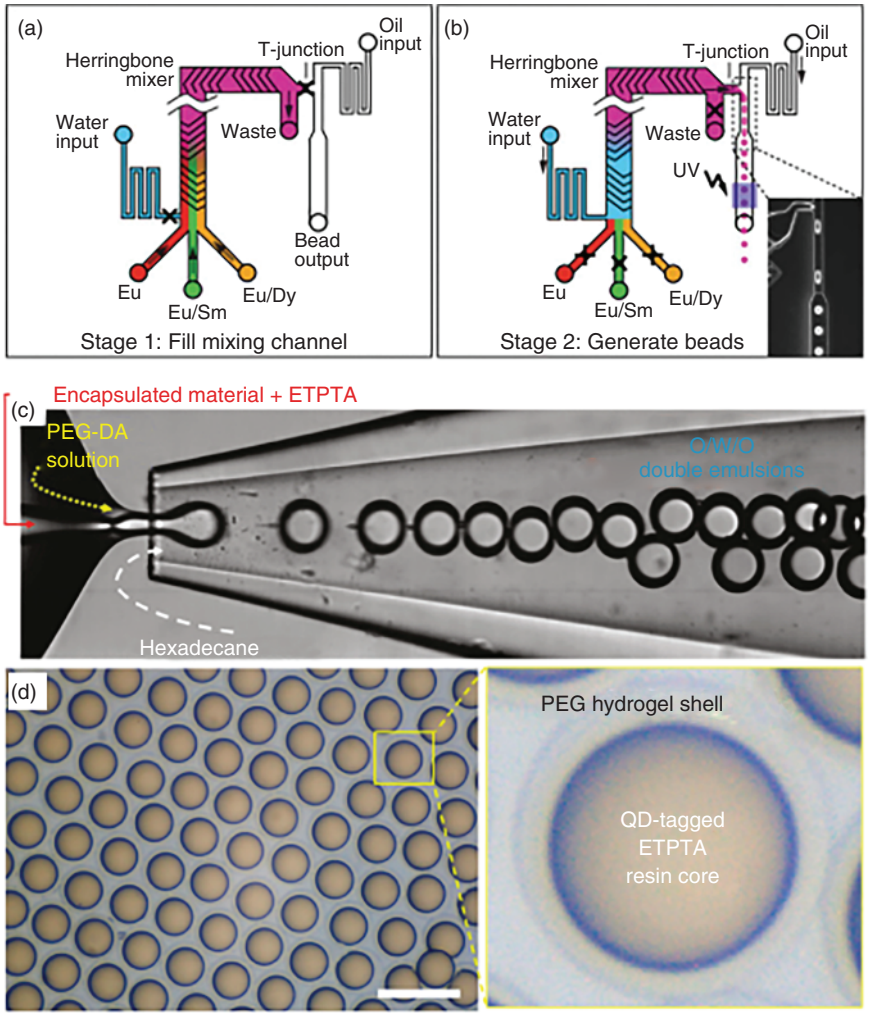

Figure 1.11 (a, b) Microfluidic bead synthesizer: (a) mixtures of lanthanide suspended in prepolymer bead mixture flowed into a microfluidic device at controlled ratios and were mixed on chip using a staggered herringbone mixer; (b) water pushed the lanthanide mixture toward a T-junction containing a continuously flowing oil stream, producing droplets, and were then polymerized into beads via illumination with UV light (b). Adapted with permission from Gerver et al. [155]. Copyright 2012, Royal Society of Chemistry. (c, d) Formation of O/W/O double emulsions in a glass microcapillary device (c); optical micrograph of the polymerized double emulsions with PEG hydrogel shells and QD-tagged ETPTA resin cores. Scale bar is 100 μm (d). Source: Adapted with permission from Zhao et al. [156]. Copyright 2011, American Chemical Society. (e) Schematic illustration of the microfluidic emulsification process and concentration and self-assembly of water-extraction-derived colloidal NPs into a hollow spherical PhC shell on the inner wall of the microcapsules. Adapted with permission from Shang et al. [157]. Copyright 2015, American Chemical Society.

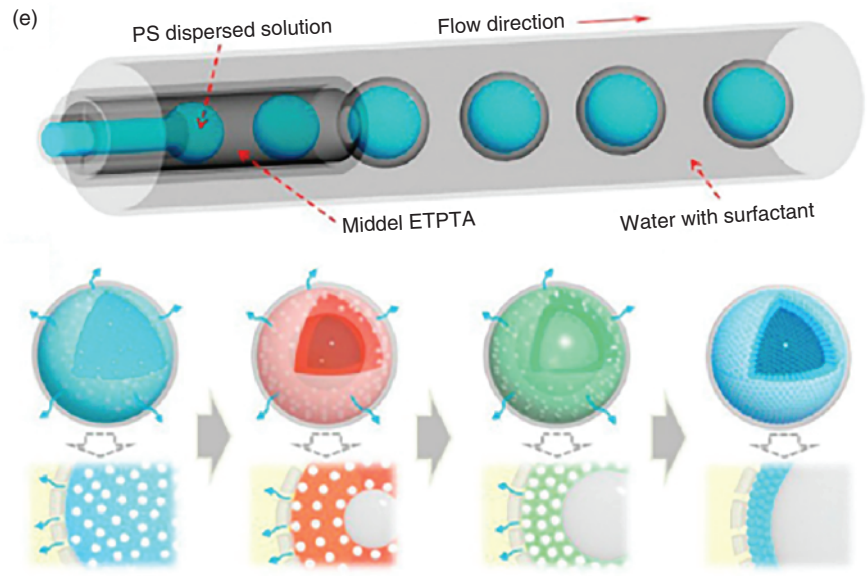

Figure 1.11 (*Continued*)

with different structural periods or different refractive indices, a series of PhC particles with different diffraction peak positions can be obtained for encoding. Unlike the fluorescence, the spectra of the PhCs originate from the reflection of their physical structures. Thus, they are resistant to photobleaching or photoquenching, which makes them a kind of ideal color-encoding element. PhCs can also be incorporated into microfluidic droplets for generating barcode particles. Shang et al. presented a new type of barcode particle with a semipermeable membrane shell and a colloidal-NP-encapsulated liquid core, using droplet microfluidics [157]. By dispersing the microcapsules in an ethanol solution to extract water from the core, their encapsulated colloidal NPs could be gradually concentrated and self-assembled into the hollow spherical PhC shell on the inner wall of the microcapsules, as schematically shown in Figure 1.11e. The resultant PhC microbubbles were composed of an outer transparent polymeric shell, a middle PhC shell, and an inner bubble core. The encoded elements of the particles originated from their PhC structure with a coated shell, which not only improved the stability of the codes but also provided a flexible surface for bioassays. In addition, by using multicompartmental PhC microbubbles, the barcode particles allowed for a substantial number of coding levels and controllable movement in multiplexing applications. More importantly, as the size of the encapsulated core and the corresponding bubbles of the barcode particles could be tailored in their emulsification process, the overall density of the PhC microbubbles could be adjusted to match the density of a detection solution so that they remained in suspension. These features made the PhC microbubbles excellent functional barcode particles in biomedical applications.

1.5 Conclusion and Perspectives

This part summarizes recent research progress on the synthesis of MMs/NMs based on droplet microfluidics and their applications in various fields. In the past decade, with the development of microchip preparation technology, materials engineered from microfluidic technologies have experienced transition from simplicity to complexity in material structure and simplification to diversity in material function, which largely compensates for the limitation of conventional synthesis methods. Based on the flexibility and integration of microfluidic manipulation, preparation of functional materials has extended from the original single emulsion droplet method to complex multiple emulsion droplet method. The resultant materials have developed from simple solid MPs to specially shaped MMs, Janus particles, porous particles, and core–shell-structured particles. A series of novel NMs has also been developed in the microfluidic system. These MMs/NMs have shown great potentials in a broad range of applications, such as drug carrier, cell encapsulation, TE, and analytical application.

Because of the theoretical research and technological innovations, droplet microfluidics currently bears significant value in an extremely wide range of areas. Despite a lot of exciting and compelling developments, there remain challenges that pose a gap between academic proof-of-concept studies and practical techniques for addressing real-world problems. Therefore, several important issues need to be solved to achieve the wide applicability of droplet microfluidics. Firstly, since current works mostly adopt single channel as the reaction unit, the yield of microfluidic synthetic materials is low compared to conventional batch mode. However, mass production is an inevitable topic to bring droplet microfluidics out of the laboratory as an industrialized technology. Fortunately, there is already some research on the scale-up of droplet microfluidic platforms, based on coaxial annular interfaces, stacking multiple generator layers, and parallel multiple modular reactors [160, 161]. The second issue is about technology promotion. The current droplet systems are usually run in specialized academic laboratories, which restrict the access to microfluidics for nonexperts. Regarding this, much effort should be paid to the simplification and modularization of basic functional units, and automation control should be enhanced to reduce manual operation. It is also important for the technology holders to actively cooperate with the researchers of clinical, medical, food, and environment topics and get their authority recognized. In other words, the microfluidic materials have bright market prospects, but the realization of their commercial value still requires the efforts of researchers and entrepreneurs. Third, much emphasis should be put on designing novel materials with more applications. For analytical application, millions of barcodes have been designed by using droplet microfluidics. However, these numbers mean little in biological applications. The main reason is that the largest multiplicity in protein detection is in the hundreds and this will be further limited by nonspecific reactions because of the cross-reaction of antibodies. Meanwhile, for gene analysis, the production of so many barcode particles is time consuming, and the size of these microfluidic

particles is relatively large, which might require the use of a large number of samples. Therefore, in the future, microfluidic material design and preparation should be application targeted and oriented. Finally, compared with the MMs, the diversity and functionalities of the droplet microfluidics-derived NMs are still lacking. For NM synthesis, purification and extraction processes, which are easily achievable in conventional approaches, should be improved in microfluidic platforms. In addition, the integration and development of online analytical methods with the microfluidic approach will significantly improve the synthesis performance by optimizing processes with an immediate feedback control. It is envisioned that, with further endeavors, droplet microfluidics is expected to be a promising platform to optimize and tailor NMs for different applications.

In conclusion, droplet microfluidics has evolved into a powerful technique and possesses application values cutting across multiple fields and disciplines. However, a lot of effort is still needed to overcome existing challenges. In particular, in-depth collaborative efforts and communication from different areas should be aimed to bridge the gap between material synthesis and applications. After addressing the issues described above, we firmly believe that more exciting accomplishments will be achieved in droplet microfluidics.

References

1 Nge, P.N., Rogers, C.I., and Woolley, A.T. (2013). Advances in microfluidic materials, functions, integration, and applications. *Chem. Rev.* 113 (4): 2550–2583.

2 Marre, S. and Jensen, K.F. (2010). Synthesis of micro and nanostructures in microfluidic systems. *Chem. Soc. Rev.* 39 (3): 1183–1202.

3 Elvira, K.S., Casadevall i Solvas, X., Wootton, R.C., and deMello, A.J. (2013). The past, present and potential for microfluidic reactor technology in chemical synthesis. *Nat. Chem.* 5 (11): 905–915.

4 Wang, X.H., Liu, J.F., Wang, P.Z. et al. (2018). Synthesis of biomaterials utilizing microfluidic technology. *Genes* 9 (6): 283.

5 Hayat, Z. and El Abed, A.I. (2018). High-throughput optofluidic acquisition of microdroplets in microfluidic systems. *Micromachines* 9 (4): 183.

6 Kaminski, T.S. and Garstecki, P. (2017). Controlled droplet microfluidic systems for multistep chemical and biological assays. *Chem. Soc. Rev.* 46 (20): 6210–6226.

7 Gong, X., Wang, Y.W., Ihli, J. et al. (2015). The crystal hotel: a microfluidic approach to biomimetic crystallization. *Adv. Mater.* 27 (45): 7395–7400.

8 Gijs, M.A., Lacharme, F., and Lehmann, U. (2010). Microfluidic applications of magnetic particles for biological analysis and catalysis. *Chem. Rev.* 110 (3): 1518–1563.

9 Nguyen, N.T., Hejazian, M., Ooi, C.H., and Kashaninejad, N. (2017). Recent advances and future perspectives on microfluidic liquid handling. *Micromachines* 8 (6): 186.

10 Gholizadeh, S., Shehata Draz, M., Zarghooni, M. et al. (2017). Microfluidic approaches for isolation, detection, and characterization of extracellular vesicles: current status and future directions. *Biosens. Bioelectron.* 91: 588–605.

11 Wang, W., Zhang, M.J., and Chu, L.Y. (2014). Functional polymeric microparticles engineered from controllable microfluidic emulsions. *Acc. Chem. Res.* 47 (2): 373–384.

12 Tumarkin, E. and Kumacheva, E. (2009). Microfluidic generation of microgels from synthetic and natural polymers. *Chem. Soc. Rev.* 38 (8): 2161–2168.

13 Lee, S.S., Kim, B., Kim, S.K. et al. (2015). Robust microfluidic encapsulation of cholesteric liquid crystals toward photonic ink capsules. *Adv. Mater.* 27 (4): 627–633.

14 Mei, L., Jin, M., Xie, S. et al. (2018). A simple capillary-based open microfluidic device for size on-demand high-throughput droplet/bubble/microcapsule generation. *Lab Chip* https://doi.org/10.1039/c8lc00479j.

15 Ferreira, J., Castro, F., Rocha, F., and Kuhn, S. (2018). Protein crystallization in a droplet-based microfluidic device: hydrodynamic analysis and study of the phase behaviour. *Chem. Eng. Sci.* 191: 232–244.

16 Caggioni, M., Traini, D., Young, P.M., and Spicer, P.T. (2018). Microfluidic production of endoskeleton droplets with controlled size and shape. *Powder Technol.* 329: 129–136.

17 Shang, L., Cheng, Y., and Zhao, Y. (2017). Emerging droplet microfluidics. *Chem. Rev.* 117 (12): 7964–8040.

18 Jiao, Y., Liu, Y., Luo, D. et al. (2018). Microfluidic-assisted fabrication of clay microgels for cell-free protein synthesis. *ACS Appl. Mater. Interfaces* https://doi.org/10.1021/acsami.8b09324.

19 Vladisavljevic, G.T., Kobayashi, I., and Nakajima, M. (2012). Production of uniform droplets using membrane, microchannel and microfluidic emulsification devices. *Microfluid. Nanofluid.* 13 (1): 151–178.

20 Ma, J.Y., Wang, Y.C., and Liu, J. (2017). Biomaterials meet microfluidics: from synthesis technologies to biological applications. *Micromachines* 8 (8): 255.

21 Abate, A.R. and Weitz, D.A. (2009). High-order multiple emulsions formed in poly(dimethylsiloxane) microfluidics. *Small* 5 (18): 2030–2032.

22 Chu, L.Y., Utada, A.S., Shah, R.K. et al. (2007). Controllable monodisperse multiple emulsions. *Angew. Chem. Int. Ed.* 46 (47): 8970–8974.

23 Ceylan, H., Yasa, I.C., and Sitti, M. (2017). 3D chemical patterning of micromaterials for encoded functionality. *Adv. Mater.* 29 (9): 1605072.

24 Leijten, J., Rouwkema, J., Zhang, Y.S. et al. (2016). Advancing tissue engineering: a tale of nano-, micro-, and macroscale integration. *Small* 12 (16): 2130–2145.

25 Lash, M.H., Jordan, J.C., Blevins, L.C. et al. (2015). Non-Brownian particle-based materials with microscale and nanoscale hierarchy. *Angew. Chem. Int. Ed.* 54 (20): 5854–5858.

26 Ghanbarzadeh, B., Oleyaei, S.A., and Almasi, H. (2015). Nanostructured materials utilized in biopolymer-based plastics for food packaging applications. *Crit. Rev. Food Sci. Nutr.* 55 (12): 1699–1723.

27 Laval, C., Bouchaudy, A., and Salmon, J.B. (2016). Fabrication of microscale materials with programmable composition gradients. *Lab Chip* 16 (7): 1234–1242.

28 Li, F., Du, M., and Zheng, Q. (2016). Dopamine/silica nanoparticle assembled, microscale porous structure for versatile superamphiphobic coating. *ACS Nano* 10 (2): 2910–2921.

29 Peng, F., Su, Y., Zhong, Y. et al. (2014). Silicon nanomaterials platform for bioimaging, biosensing, and cancer therapy. *Acc. Chem. Res.* 47 (2): 612–623.

30 Makgwane, P.R. and Ray, S.S. (2014). Synthesis of nanomaterials by continuous-flow microfluidics: a review. *J. Nanosci. Nanotechnol.* 14 (2): 1338–1363.

31 Shiba, K. and Ogawa, M. (2018). Precise synthesis of well-defined inorganic–organic hybrid particles. *Chem. Rec.* 18: 950–968.

32 Stolzenburg, P., Lorenz, T., Dietzel, A., and Garnweitner, G. (2018). Microfluidic synthesis of metal oxide nanoparticles via the nonaqueous method. *Chem. Eng. Sci.* 191: 500–510.

33 Sun, L., Wang, J., Yu, Y. et al. (2018). Graphene oxide hydrogel particles from microfluidics for oil decontamination. *J. Colloid Interface Sci.* 528: 372–378.

34 Connacher, W., Zhang, N., Huang, A. et al. (2018). Micro/nano acoustofluidics: materials, phenomena, design, devices, and applications. *Lab Chip* 18 (14): 1952–1996.

35 Liu, Y. and Jiang, X. (2017). Why microfluidics? Merits and trends in chemical synthesis. *Lab Chip* 17 (23): 3960–3978.

36 Liu, Z.M., Yang, Y., Du, Y., and Pang, Y. (2017). Advances in droplet-based microfluidic technology and its applications. *Chin. J. Anal. Chem.* 45 (2): 282–295.

37 McClements, D.J. (2018). Encapsulation, protection, and delivery of bioactive proteins and peptides using nanoparticle and microparticle systems: a review. *Adv. Colloid Interface Sci.* 253: 1–22.

38 Naghizadeh, Z., Karkhaneh, A., and Khojasteh, A. (2018). Simultaneous release of melatonin and methylprednisolone from an injectable in situ self-crosslinked hydrogel/microparticle system for cartilage tissue engineering. *J. Biomed. Mater. Res. A* 106 (7): 1932–1940.

39 Chaurasiya, B., Huang, L., Du, Y. et al. (2018). Size-based anti-tumoral effect of paclitaxel loaded albumin microparticle dry powders for inhalation to treat metastatic lung cancer in a mouse model. *Int. J. Pharm.* 542: 90–99.

40 Rodríguez Villanueva, J. and Rodríguez Villanueva, L. (2017). Turning the screw even further to increase microparticle retention and ocular bioavailability of associated drugs: the bioadhesion goal. *Int. J. Pharm.* 531 (1): 167–178.

41 Mooberry, M.J. and Key, N.S. (2016). Microparticle analysis in disorders of hemostasis and thrombosis. *Cytometry, Part A* 89 (2): 111–122.

42 Jy, W., Horstman, L.L., and Ahn, Y.S. (2010). Microparticle size and its relation to composition, functional activity, and clinical significance. *Semin. Thromb. Hemost.* 36 (8): 876–880.

43 Zhang, L., Yang, W., Hu, C. et al. (2018). Properties and applications of nanoparticle/microparticle conveyors with adjuvant characteristics suitable for oral vaccination. *Int. J. Nanomed.* 13: 2973–2987.

44 Ghosh Dastidar, D., Saha, S., and Chowdhury, M. (2018). Porous microspheres: synthesis, characterisation and applications in pharmaceutical & medical fields. *Int. J. Pharm.* 548 (1): 34–48.

45 Wong, C.Y., Al-Salami, H., and Dass, C.R. (2018). Microparticles, microcapsules and microspheres: a review of recent developments and prospects for oral delivery of insulin. *Int. J. Pharm.* 537: 223–244.

46 Lee, B.K., Yun, Y., and Park, K. (2016). PLA micro- and nano-particles. *Adv. Drug Deliv. Rev.* 107: 176–191.

47 Li, W., Zhang, L., Ge, X. et al. (2018). Microfluidic fabrication of microparticles for biomedical applications. *Chem. Soc. Rev.* 47 (15): 5646–5683.

48 Yeo, S.J., Park, K.J., Guo, K. et al. (2016). Microfluidic generation of monodisperse and photoreconfigurable microspheres for floral iridescence-inspired structural colorization. *Adv. Mater.* 28 (26): 5268–5275.

49 Cui, J., Björnmalm, M., Liang, K. et al. (2014). Super-soft hydrogel particles with tunable elasticity in a microfluidic blood capillary model. *Adv. Mater.* 26 (43): 7295–7299.

50 Seth, A., Béalle, G., Santanach-Carreras, E. et al. (2012). Design of vesicles using capillary microfluidic devices: from magnetic to multifunctional vesicles. *Adv. Mater.* 24 (26): 3544–3548.

51 Deng, N.N., Yelleswarapu, M., Zheng, L., and Huck, W.T. (2017). Microfluidic assembly of monodisperse vesosomes as artificial cell models. *J. Am. Chem. Soc.* 139 (2): 587–590.

52 Abate, A.R., Kutsovsky, M., Seiffert, S. et al. (2011). Synthesis of monodisperse microparticles from non-Newtonian polymer solutions with microfluidic devices. *Adv. Mater.* 23 (15): 1757–1760.

53 Arcos-Turmo, I., Herrada, M.A., Lopez-Herrera, J.M. et al. (2018). Novel swirl flow-focusing microfluidic device for the production of monodisperse microbubbles. *Microfluid. Nanofluid.* 22 (8): 79.

54 Liang, S.S., Li, J., Li, X.M. et al. (2018). Microfluidic fabrication of ceramic microspheres with controlled morphologies. *J. Am. Ceram. Soc.* 101 (9): 3787–3796.

55 Visaveliya, N. and Kohler, J.M. (2015). Simultaneous size and color tuning of polymer microparticles in a single-step microfluidic synthesis: particles for fluorescence labeling. *J. Mater. Chem. C* 3 (4): 844–853.

56 Liu, H., Qian, X., Wu, Z.J. et al. (2016). Microfluidic synthesis of QD-encoded PEGDA microspheres for suspension assay. *J. Mater. Chem. B* 4 (3): 482–488.

57 Jeong, W.J., Kim, J.Y., Choo, J. et al. (2005). Continuous fabrication of biocatalyst immobilized microparticles using photopolymerization and immiscible liquids in microfluidic systems. *Langmuir* 21 (9): 3738–3741.

58 Tan, W.H. and Takeuchi, S. (2007). Monodisperse alginate hydrogel microbeads for cell encapsulation. *Adv. Mater.* 19 (18): 2696–2701.

59 Yadavali, S., Jeong, H.H., Lee, D., and Issadore, D. (2018). Silicon and glass very large scale microfluidic droplet integration for terascale generation of polymer microparticles. *Nat. Commun.* 9 (1): 1222.

60 Nisisako, T., Torii, T., Takahashi, T., and Takizawa, Y. (2006). Synthesis of monodisperse bicolored Janus particles with electrical anisotropy using a microfluidic co-flow system. *Adv. Mater.* 18 (9): 1152.

61 Liu, M., Sun, X.T., Yang, C.G., and Xu, Z.R. (2016). On-chip preparation of calcium alginate particles based on droplet templates formed by using a centrifugal microfluidic technique. *J. Colloid Interface Sci.* 466: 20–27.

62 Velasco, D., Tumarkin, E., and Kumacheva, E. (2012). Microfluidic encapsulation of cells in polymer microgels. *Small* 8 (11): 1633–1642.

63 Utech, S., Prodanovic, R., Mao, A.S. et al. (2015). Microfluidic generation of monodisperse, structurally homogeneous alginate microgels for cell encapsulation and 3D cell culture. *Adv. Healthc. Mater.* 4 (11): 1628–1633.

64 Jeong, H.H., Yadavali, S., Issadore, D., and Lee, D. (2017). Liter-scale production of uniform gas bubbles via parallelization of flow-focusing generators. *Lab Chip* 17 (15): 2667–2673.

65 Ofner, A., Moore, D.G., Ruhs, P.A. et al. (2017). High-throughput step emulsification for the production of functional materials using a glass microfluidic device. *Macromol. Chem. Phys.* 218 (2): 1600472.

66 Lee, K.J., Yoon, J., and Lahann, J. (2011). Recent advances with anisotropic particles. *Curr. Opin. Colloid Interface Sci.* 16 (3): 195–202.

67 Sun, X.T., Yang, C.G., and Xu, Z.R. (2016). Controlled production of size-tunable Janus droplets for submicron particle synthesis using an electrospray microfluidic chip. *RSC Adv.* 6 (15): 12042–12047.

68 Li, S.S., Yu, X.L., You, S.J. et al. (2014). Generation of $BiFeO_3$-Fe_3O_4 Janus particles based on droplet microfluidic method. *Appl. Phys. Lett.* 105 (4): 042903.

69 Nisisako, T. (2016). Recent advances in microfluidic production of Janus droplets and particles. *Curr. Opin. Colloid Interface Sci.* 25: 1–12.

70 Teh, S.Y., Lin, R., Hung, L.H., and Lee, A.P. (2008). Droplet microfluidics. *Lab Chip* 8 (2): 198–220.

71 Serra, C.A. and Chang, Z.Q. (2008). Microfluidic-assisted synthesis of polymer particles. *Chem. Eng. Technol.* 31 (8): 1099–1115.

72 Haeberle, S., Naegele, L., Burger, R. et al. (2008). Alginate bead fabrication and encapsulation of living cells under centrifugally induced artificial gravity conditions. *J. Microencapsulation* 25 (4): 267–274.

73 Choi, C.H., Weitz, D.A., and Lee, C.S. (2013). One step formation of controllable complex emulsions: from functional particles to simultaneous encapsulation of hydrophilic and hydrophobic agents into desired position. *Adv. Mater.* 25 (18): 2536–2541.

74 Haase, M.F. and Brujic, J. (2014). Tailoring of high-order multiple emulsions by the liquid-liquid phase separation of ternary mixtures. *Angew. Chem. Int. Ed.* 53 (44): 11793–11797.

75 Choi, C.H., Kim, J., Nam, J.O. et al. (2014). Microfluidic design of complex emulsions. *ChemPhysChem* 15 (1): 21–29.

76 Deng, N.N., Wang, W., Ju, X.J. et al. (2013). Wetting-induced formation of controllable monodisperse multiple emulsions in microfluidics. *Lab Chip* 13 (20): 4047–4052.

77 Jeong, G.Y., Ricco, R., Liang, K. et al. (2015). Bioactive MIL-88A framework hollow spheres via interfacial reaction in-droplet microfluidics for enzyme and nanoparticle encapsulation. *Chem. Mater.* 27 (23): 7903–7909.

78 Hennequin, Y., Pannacci, N., de Torres, C.P. et al. (2009). Synthesizing microcapsules with controlled geometrical and mechanical properties with microfluidic double emulsion technology. *Langmuir* 25 (14): 7857–7861.

79 Ren, P.W., Ju, X.J., Xie, R., and Chu, L.Y. (2010). Monodisperse alginate microcapsules with oil core generated from a microfluidic device. *J. Colloid Interface Sci.* 343 (1): 392–395.

80 Montazeri, L., Bonakdar, S., Taghipour, M. et al. (2016). Modification of PDMS to fabricate PLGA microparticles by a double emulsion method in a single microfluidic device. *Lab Chip* 16 (14): 2596–2600.

81 Amstad, E., Kim, S.H., and Weitz, D.A. (2012). Photo- and thermo-responsive polymersomes for triggered release. *Angew. Chem. Int. Ed.* 51 (50): 12499–12503.

82 Mou, C.L., Ju, X.J., Zhang, L. et al. (2014). Monodisperse and fast-responsive poly(*N*-isopropylacrylamide) microgels with open-celled porous structure. *Langmuir* 30 (5): 1455–1464.

83 Costantini, M., Guzowski, J., Zuk, P.J. et al. (2018). Electric field assisted microfluidic platform for generation of tailorable porous microbeads as cell carriers for tissue engineering. *Adv. Funct. Mater.* 28 (32): 1870223.

84 Wang, J., Shang, L., Cheng, Y. et al. (2015). Microfluidic generation of porous particles encapsulating spongy graphene for oil absorption. *Small* 11 (32): 3890–3895.

85 Maeda, K., Onoe, H., Takinoue, M., and Takeuchi, S. (2012). Controlled synthesis of 3D multicompartmental particles with centrifuge-based microdroplet formation from a multi-barreled capillary. *Adv. Mater.* 24 (10): 1340–1346.

86 Kim, S.H., Shum, H.C., Kim, J.W. et al. (2011). Multiple polymersomes for programmed release of multiple components. *J. Am. Chem. Soc.* 133 (38): 15165–15171.

87 Zhou, M.M., Shen, L., Lin, X. et al. (2017). Design and pharmaceutical applications of porous particles. *RSC Adv.* 7 (63): 39490–39501.

88 Wan, J., Bick, A., Sullivan, M., and Stone, H.A. (2008). Controllable microfluidic production of microbubbles in water-in-oil emulsions and the formation of porous microparticles. *Adv. Mater.* 20 (17): 3314.

89 Geng, Y., Dalhaimer, P., Cai, S. et al. (2007). Shape effects of filaments versus spherical particles in flow and drug delivery. *Nat. Nanotechnol.* 2 (4): 249–255.

90 Fish, M.B., Thompson, A.J., Fromen, C.A., and Eniola-Adefeso, O. (2015). Emergence and utility of nonspherical particles in biomedicine. *Ind. Eng. Chem. Res.* 54 (16): 4043–4059.

91 Peyer, K.E., Zhang, L., and Nelson, B.J. (2013). Bio-inspired magnetic swimming microrobots for biomedical applications. *Nanoscale* 5 (4): 1259–1272.

92 Xu, S., Nie, Z., Seo, M. et al. (2005). Generation of monodisperse particles by using microfluidics: control over size, shape, and composition. *Angew. Chem. Int. Ed.* 44 (5): 724–728.

93 Wang, W., He, X.H., Zhang, M.J. et al. (2017). Controllable microfluidic fabrication of microstructured materials from nonspherical particles to helices. *Macromol. Rapid Commun.* 38 (23): 1700429.

94 Lin, Y.S., Yang, C.H., Hsu, Y.Y., and Hsieh, C.L. (2013). Microfluidic synthesis of tail-shaped alginate microparticles using slow sedimentation. *Electrophoresis* 34 (3): 425–431.

95 Nisisako, T. and Torii, T. (2007). Formation of biphasic Janus droplets in a microfabricated channel for the synthesis of shape-controlled polymer microparticles. *Adv. Mater.* 19 (11): 1489–1493.

96 Luo, Z., Xu, Y., Ye, E. et al. (2018). Recent progress in macromolecule-anchored hybrid gold nanomaterials for biomedical applications. *Macromol. Rapid Commun.* https://doi.org/10.1002/marc.201800029.

97 Lin, Y.J., Gao, Y., Fang, F., and Fan, Z.Y. (2018). Recent progress on printable power supply devices and systems with nanomaterials. *Nano Res.* 11 (6): 3065–3087.

98 Cui, L., Li, C.C., Tang, B., and Zhang, C.Y. (2018). Advances in the integration of quantum dots with various nanomaterials for biomedical and environmental applications. *Analyst* 143 (11): 2469–2478.

99 Qi, G.B., Gao, Y.J., Wang, L., and Wang, H. (2018). Self-assembled peptide-based nanomaterials for biomedical imaging and therapy. *Adv. Mater.* 30 (22): e1703444.

100 Li, L.L., Li, X.D., and Wang, H. (2017). Microfluidic synthesis of nanomaterials for biomedical applications. *Small Methods* 1 (8): 1700140.

101 Macchione, M.A., Biglione, C., and Strumia, M. (2018). Design, synthesis and architectures of hybrid nanomaterials for therapy and diagnosis applications. *Polymers* 10 (5): 527.

102 Ma, J., Lee, S.M., Yi, C., and Li, C.W. (2017). Controllable synthesis of functional nanoparticles by microfluidic platforms for biomedical applications - a review. *Lab Chip* 17 (2): 209–226.

103 Jung, J.H., Park, T.J., Lee, S.Y., and Seo, T.S. (2012). Homogeneous biogenic paramagnetic nanoparticle synthesis based on a microfluidic droplet generator. *Angew. Chem. Int. Ed.* 51 (23): 5634–5637.

104 Zhang, L., Feng, Q., Wang, J. et al. (2015). Microfluidic synthesis of hybrid nanoparticles with controlled lipid layers: understanding flexibility-regulated cell-nanoparticle interaction. *ACS Nano* 9 (10): 9912–9921.

105 Ran, R., Wang, H., Liu, Y. et al. (2018). Microfluidic self-assembly of a combinatorial library of single- and dual-ligand liposomes for in vitro and in vivo tumor targeting. *Eur. J. Pharm. Biopharm.* 130: 1–10.

106 Ortiz de Solorzano, I., Prieto, M., Mendoza, G. et al. (2016). Microfluidic synthesis and biological evaluation of photothermal biodegradable copper sulfide nanoparticles. *ACS Appl. Mater. Interfaces* 8 (33): 21545–21554.

107 Phillips, T.W., Lignos, I.G., Maceiczyk, R.M. et al. (2014). Nanocrystal synthesis in microfluidic reactors: where next? *Lab Chip* 14 (17): 3172–3180.

108 Nightingale, A.M. and Demello, J.C. (2013). Segmented flow reactors for nanocrystal synthesis. *Adv. Mater.* 25 (13): 1813–1821.

109 McMullen, J.P. and Jensen, K.F. (2010). Integrated microreactors for reaction automation: new approaches to reaction development. *Annu. Rev. Anal. Chem. (Palo Alto Calif)* 3: 19–42.

110 Lazarus, L.L., Riche, C.T., Marin, B.C. et al. (2012). Two-phase microfluidic droplet flows of ionic liquids for the synthesis of gold and silver nanoparticles. *ACS Appl. Mater. Interfaces* 4 (6): 3077–3083.

111 Shestopalov, I., Tice, J.D., and Ismagilov, R.F. (2004). Multi-step synthesis of nanoparticles performed on millisecond time scale in a microfluidic droplet-based system. *Lab Chip* 4 (4): 316–321.

112 Gu, T., Zheng, C., He, F. et al. (2018). Electrically controlled mass transport into microfluidic droplets from nanodroplet carriers with application in controlled nanoparticle flow synthesis. *Lab Chip* 18 (9): 1330–1340.

113 Song, H., Chen, D.L., and Ismagilov, R.F. (2006). Reactions in droplets in microfluidic channels. *Angew. Chem. Int. Ed.* 45 (44): 7336–7356.

114 Theberge, A.B., Courtois, F., Schaerli, Y. et al. (2010). Microdroplets in microfluidics: an evolving platform for discoveries in chemistry and biology. *Angew. Chem. Int. Ed.* 49 (34): 5846–5868.

115 Rhee, M., Valencia, P.M., Rodriguez, M.I. et al. (2011). Synthesis of size-tunable polymeric nanoparticles enabled by 3D hydrodynamic flow focusing in single-layer microchannels. *Adv. Mater.* 23 (12): 79–83.

116 Alam, M.P., Jagodzinska, B., Campagna, J. et al. (2016). C—O bond formation in a microfluidic reactor: high yield S_NAr substitution of heteroaryl chlorides. *Tetrahedron Lett.* 57 (19): 2059–2062.

117 Capretto, L., Carugo, D., Mazzitelli, S. et al. (2013). Microfluidic and lab-on-a-chip preparation routes for organic nanoparticles and vesicular systems for nanomedicine applications. *Adv. Drug Deliv. Rev.* 65: 1496–1532.

118 Su, Y.F., Kim, H., Kovenklioglu, S., and Lee, W.Y. (2007). Continuous nanoparticle production by microfluldic-based emulsion, mixing and crystallization. *J. Solid State Chem.* 180 (9): 2625–2629.

119 Hung, L.H., Teh, S.Y., Jester, J., and Lee, A.P. (2010). PLGA micro/nanosphere synthesis by droplet microfluidic solvent evaporation and extraction approaches. *Lab Chip* 10 (14): 1820–1825.

120 Faustini, M., Kim, J., Jeong, G.Y. et al. (2013). Microfluidic approach toward continuous and ultrafast synthesis of metal–organic framework crystals and hetero structures in confined microdroplets. *J. Am. Chem. Soc.* 135 (39): 14619–14626.

121 Wang, C.W., Oskooei, A., Sinton, D., and Moffitt, M.G. (2010). Controlled self-assembly of quantum dot-block copolymer colloids in multiphase microfluidic reactors. *Langmuir* 26 (2): 716–723.

122 Liu, B.T., Vellingiri, K., Jo, S.H. et al. (2018). Recent advances in controlled modification of the size and morphology of metal–organic frameworks. *Nano Res.* 11 (9): 4441–4467.

123 Lu, K., Aung, T., Guo, N. et al. (2018). Nanoscale metal–organic frameworks for therapeutic, imaging, and sensing applications. *Adv. Mater.* https://doi.org/10.1002/adma.201707634.

124 Liu, D., Zhang, H., Fontana, F. et al. (2017). Microfluidic-assisted fabrication of carriers for controlled drug delivery. *Lab Chip* 17 (11): 1856–1883.

125 Hasani-Sadrabadi, M.M., Taranejoo, S., Dashtimoghadam, E. et al. (2016). Microfluidic manipulation of core/shell nanoparticles for oral delivery of chemotherapeutics: a new treatment approach for colorectal cancer. *Adv. Mater.* 28 (21): 4134–4141.

126 Zhang, H., Liu, D., Shahbazi, M.A. et al. (2014). Fabrication of a multifunctional nano-in-micro drug delivery platform by microfluidic templated encapsulation of porous silicon in polymer matrix. *Adv. Mater.* 26 (26): 4497–4503.

127 Sanjay, S.T., Zhou, W., Dou, M. et al. (2018). Recent advances of controlled drug delivery using microfluidic platforms. *Adv. Drug Deliv. Rev.* 128: 3–28.

128 Hasani-Sadrabadi, M.M., Karimkhani, V., Majedi, F.S. et al. (2014). Microfluidic-assisted self-assembly of complex dendritic polyethylene drug delivery nanocapsules. *Adv. Mater.* 26 (19): 3118–3123.

129 Xu, Q., Hashimoto, M., Dang, T.T. et al. (2009). Preparation of monodisperse biodegradable polymer microparticles using a microfluidic flow-focusing device for controlled drug delivery. *Small* 5 (13): 1575–1581.

130 Li, Y.N., Yan, D., Fu, F.F. et al. (2017). Composite core-shell microparticles from microfluidics for synergistic drug delivery. *Sci. China Mater.* 60 (6): 543–553.

131 Wei, J., Ju, X.J., Zou, X.Y. et al. (2014). Multi-stimuli-responsive microcapsules for adjustable controlled-release. *Adv. Funct. Mater.* 24 (22): 3312–3323.

132 Molinaro, R., Evangelopoulos, M., Hoffman, J.R. et al. (2018). Design and development of biomimetic nanovesicles using a microfluidic approach. *Adv. Mater.* 30 (15): e1702749.

133 Feng, Q., Zhang, L., Liu, C. et al. (2015). Microfluidic based high throughput synthesis of lipid-polymer hybrid nanoparticles with tunable diameters. *Biomicrofluidics* 9 (5): 052604.

134 Fontana, F., Shahbazi, M.A., Liu, D. et al. (2017). Multistaged nanovaccines based on porous silicon@acetalated dextran@cancer cell membrane for cancer immunotherapy. *Adv. Mater.* 29 (7): 1603239.

135 Wieduwild, R., Krishnan, S., Chwalek, K. et al. (2015). Noncovalent hydrogel beads as microcarriers for cell culture. *Angew. Chem. Int. Ed.* 54 (13): 3962–3966.

136 Allazetta, S., Kolb, L., Zerbib, S. et al. (2015). Cell-instructive microgels with tailor-made physicochemical properties. *Small* 11 (42): 5647–5656.

137 Kapourani, E., Neumann, F., Achazi, K. et al. (2018). Droplet-based microfluidic templating of polyglycerol-based microgels for the encapsulation of cells: a comparative study. *Macromol. Biosci.* 18 (10): 1800116.

138 Zhou, X.C., Haraldsson, T., Nania, S. et al. (2018). Human cell encapsulation in gel microbeads with cosynthesized concentric nanoporous solid shells. *Adv. Funct. Mater.* 28 (21): 1707129.

139 Agarwal, P., Zhao, S., Bielecki, P. et al. (2013). One-step microfluidic generation of pre-hatching embryo-like core-shell microcapsules for miniaturized 3D culture of pluripotent stem cells. *Lab Chip* 13 (23): 4525–4533.

140 Lutolf, M.P. and Hubbell, J.A. (2005). Synthetic biomaterials as instructive extracellular microenvironments for morphogenesis in tissue engineering. *Nat. Biotechnol.* 23 (1): 47–55.

141 Place, E.S., Evans, N.D., and Stevens, M.M. (2009). Complexity in biomaterials for tissue engineering. *Nat. Mater.* 8 (6): 457–470.

142 Salgado, A.J., Coutinho, O.P., and Reis, R.L. (2004). Bone tissue engineering: state of the art and future trends. *Macromol. Biosci.* 4 (8): 743–765.

143 Ma, P.X. (2008). Biomimetic materials for tissue engineering. *Adv. Drug Deliv. Rev.* 60 (2): 184–198.

144 Hou, Y., Xie, W., Achazi, K. et al. (2018). Injectable degradable PVA microgels prepared by microfluidic technology for controlled osteogenic differentiation of mesenchymal stem cells. *Acta Biomater.* https://doi.org/10.1016/j.actbio.2018.07.003.

145 Vardar, E., Larsson, H.M., Allazetta, S. et al. (2018). Microfluidic production of bioactive fibrin micro-beads embedded in crosslinked collagen used as an injectable bulking agent for urinary incontinence treatment. *Acta Biomater.* 67: 156–166.

146 Yu, J., Huang, T.R., Lim, Z.H. et al. (2016). Production of hollow bacterial cellulose microspheres using microfluidics to form an injectable porous scaffold for wound healing. *Adv. Healthc. Mater.* 5 (23): 2983–2992.

147 Liu, H.T., Wang, H., Wei, W.B. et al. (2018). A microfluidic strategy for controllable generation of water-in-water droplets as biocompatible microcarriers. *Small* https://doi.org/10.1002/smll.201801095.

148 Liu, Q. and Boyd, B.J. (2013). Liposomes in biosensors. *Analyst* 138 (2): 391–409.

149 Kirsch, J., Siltanen, C., Zhou, Q. et al. (2013). Biosensor technology: recent advances in threat agent detection and medicine. *Chem. Soc. Rev.* 42 (22): 8733–8768.

150 Visaveliya, N. and Köhler, J.M. (2015). Microfluidic assisted synthesis of multipurpose polymer nanoassembly particles for fluorescence, LSPR, and SERS activities. *Small* 11 (48): 6435–6443.

151 Lohse, S.E., Eller, J.R., Sivapalan, S.T. et al. (2013). A simple millifluidic benchtop reactor system for the high-throughput synthesis and functionalization of gold nanoparticles with different sizes and shapes. *ACS Nano* 7 (5): 4135–4150.

152 Knauer, A., Thete, A., Li, S. et al. (2011). Au/Ag/Au double shell nanoparticles with narrow size distribution obtained by continuous micro segmented flow synthesis. *Chem. Eng. J.* 166 (3): 1164–1169.

153 Kim, S.H., Lee, T.Y., and Lee, S.S. (2014). Osmocapsules for direct measurement of osmotic strength. *Small* 10 (6): 1155–1162.

154 Zhao, Y., Cheng, Y., Shang, L. et al. (2015). Microfluidic synthesis of barcode particles for multiplex assays. *Small* 11 (2): 151–174.

155 Gerver, R.E., Gómez-Sjöberg, R., Baxter, B.C. et al. (2012). Programmable microfluidic synthesis of spectrally encoded microspheres. *Lab Chip* 12 (22): 4716–4723.

156 Zhao, Y., Shum, H.C., Chen, H. et al. (2011). Microfluidic generation of multifunctional quantum dot barcode particles. *J. Am. Chem. Soc.* 133 (23): 8790–8793.

157 Shang, L., Fu, F., Cheng, Y. et al. (2015). Photonic crystal microbubbles as suspension barcodes. *J. Am. Chem. Soc.* 137 (49): 15533–15539.

158 Medintz, I.L., Uyeda, H.T., Goldman, E.R., and Mattoussi, H. (2005). Quantum dot bioconjugates for imaging, labelling and sensing. *Nat. Mater.* 4 (6): 435–446.

159 Pitruzzello, G. and Krauss, T.F. (2018). Photonic crystal resonances for sensing and imaging. *J. Opt.* 20 (7): 073004.

160 Liu, D., Cito, S., Zhang, Y. et al. (2015). A versatile and robust microfluidic platform toward high throughput synthesis of homogeneous nanoparticles with tunable properties. *Adv. Mater.* 27 (14): 2298–2304.

161 Huang, Y.C., Han, T.T., Xuan, J. et al. (2018). Design criteria and applications of multi-channel parallel microfluidic module. *J. Micromech. Microeng.* 28 (10): 105021.